

Low-Latency Communication using Delay-Aware Relays Against Reactive Adversaries

Vivek Chaudhary and Harshan Jagadeesh

Abstract

This work addresses a reactive jamming attack on the low-latency messages of a victim, wherein the jammer deploys countermeasure detection mechanisms to change its strategy. We highlight that the existing schemes against reactive jammers use relays with instantaneous full-duplex (FD) radios to evade the attack. However, due to the limitation of the radio architecture of the FD helper, instantaneous forwarding may not be possible in practice, thereby leading to increased decoding complexity at the destination and a high detection probability at the adversary. Pointing at this drawback, we propose a delay-aware cooperative framework wherein the victim seeks assistance from a delay-aware FD helper to forward its messages to the destination within the latency constraints. In particular, we first model the processing delay at the helper based on its hardware architecture, and then propose two low-complexity mitigation schemes, wherein the victim and the helper share their uplink frequencies using appropriate energy-splitting factors. For both the schemes, we solve the optimization problems of computing the near-optimal energy-splitting factors that minimize the joint error rates at the destination. Finally, through analytical and simulation results, we show that the proposed schemes facilitate the victim in evading the jamming attack whilst deceiving the reactive adversary.

Index Terms

Reactive adversary, low-latency communication, full-duplex radios, multiple access channels

I. INTRODUCTION

The next generation of wireless networks finds its use-cases in critical infrastructures such as vehicular networks involving autonomous vehicles [1]. Since these applications carry vital information that needs to reach the destination within a deadline, they are ideal targets for an adversary. Among the various attack models that target use-cases with deadline constraints, jamming attacks, due to their ease of execution using off-the-shelf radio devices, have been popular means of executing Denial of Service (DoS) attacks thereby forcing deadline violation on the packets. Moreover, due to recent

V. Chaudhary and H. Jagadeesh are with the Department of Electrical Engineering, Indian Institute of Technology, Delhi, 110016, India. E-mail: (chaudhary03vivek@gmail.com, jharshan@ee.iitd.ac.in)

technological advancements in radio architecture, the adversary has become more potent than its traditional counterpart. In particular, it has been shown that in addition to jamming, an adversary may monitor the network for possible countermeasures and change its attacking strategy based on the action taken by the victim. Such a class of adversaries are referred to as reactive adversaries [2], [3]. Using the recent developments in full-duplex (FD) radios [4]–[10] and cognitive radios [11]–[14], the authors in [15]–[18] presented one such adversarial model, where a reactive adversary uses FD cognitive radios to execute jamming attacks. Here, besides jamming, the adversary measures the average energy level of the jammed frequency to prevent the victim node from using state-of-art countermeasures such as, frequency hopping (FH). Also, [19] presented another class of adversarial model, wherein the reactive jamming adversary also measures the correlation between the symbols of the jammed frequency and other frequencies, thus, preventing the victim from using repetition coding across frequencies. As a first step towards mitigating the energy monitoring reactive adversary, [15]–[18] presented a decode-and-forward based cooperative countermeasure, wherein the victim uses a fraction of its energy to communicate its low-latency messages to the destination with the help of an adjacent FD helper. The helper multiplexes the victim’s symbols along with its symbols so as to facilitate the destination to jointly decode the symbols of both the nodes. Furthermore, the countermeasure is such that the victim and the helper pour their residual energies to ensure not getting detected by the adversary. We point out that the foundational assumption for the analysis in [15]–[18] is that the helper instantaneously decodes, and multiplexes the victim’s decoded symbols to the destination thereby ensuring that the messages of the victim do not violate the deadline constraint. We note that while instantaneous forwarding by the helper facilitates low-latency communication of the victim’s messages, it may not be realizable by all radio architectures due to the processing delay. This opens up questions on how to design countermeasures with practical FD radios and still ensure that the victim’s messages reach the destination within the deadline.

A. Motivation

In the countermeasure contributed by [15]–[17], it is assumed that the processing delay at the helper in forwarding the victim’s symbols is negligible. Thus, the victim’s symbols and the multiplexed symbols from the helper reach the destination during the same symbol interval. However, when using practical FD radios, the forwarding process may not be instantaneous, and the processing delay at the helper can be of the order of several symbol durations. In such cases, the symbols on the two links reach the destination during different symbol intervals, thereby yielding a signal model different from that of [15]–[17]. Moreover, if the helper decides to use multiple receive-antennas to improve the diversity order, the processing delay further increases due to additional delay contributed by the self-

interference cancellation (SIC) blocks of the FD radios [20]. Thus, using practical FD radios to combat reactive adversaries has the following three consequences: (i) The existing analysis of [15]–[17] does not hold as the symbols on the Victim-to-Destination and the Helper-to-Destination links are observed at the destination in an asynchronous fashion, (ii) Due to the processing delay, a few multiplexed symbols reach the destination after the deadline, thereby violating the low-latency constraint, and (iii) The symbols on the victim’s and the helper’s frequencies are uncoordinated in energy, resulting in fluctuations in the average energy level of both the frequencies, thereby increasing the probability of detection by the energy detector. *Thus, these limitations of the existing countermeasures motivate us to design new countermeasures that consider the helper’s practical limitations in facilitating reliable and low-latency communication of the victim’s symbols.*

B. Contributions

- 1) To facilitate reliable communication between the victim and the destination, we propose a framework wherein the victim seeks assistance from an FD helper to multiplex-and-forward its symbols to the destination in an asynchronous manner, such that the victim and the helper share the helper’s uplink frequency using an energy-splitting factor $\alpha \in (0, 1)$. We first model the processing delay at the helper using the parameter Θ which is a function of the number of receive-antennas at the helper and then propose a strategy so that the victim and the helper cooperatively use their bands to reliably communicate and still not get detected by the adversary. Since this framework incorporates the delay parameter at the helper, we refer to this framework as the Delay-Aware Semi-Coherent Multiplex-and-Forward (DASC-MF) mitigation scheme. With On-Off Keying (OOK) at the victim and M -PSK at the helper, we highlight that due to the processing delay, the symbols received across several symbol intervals at the destination are correlated. Thus, the decoding complexity of the optimal decoder is $\mathcal{O}(4M^2)$, which makes its implementation challenging. We also show that the symbols received at the destination from the victim and the helper are still uncoordinated in energy, thereby, making the proposed countermeasure susceptible to detection by the adversary. To circumvent these challenges, we propose 3ϕ DASC-MF scheme, which falls under the framework of DASC-MF as a special case. (See Sec. III)
- 2) In the 3ϕ DASC-MF scheme, we divide the frame structure into three parts, parametrized by the processing delay, Θ , such that, $\Theta \leq \frac{L}{2}$, where L denotes the number of symbols transmitted in a frame by the victim. The novel idea of this strategy is to use two energy-splitting factors, $\alpha \in (0, 1)$ and $\beta \in (0, 1)$ at different portions of the frame. Through an appropriate choice of α , we show that the correlation across the symbols can be minimized thereby ensuring that

symbols at different symbol intervals can be independently decoded and also show improved energy coordination when compared to the vanilla DASC-MF scheme. For this strategy, we provide strong analytical results on the error performance, and based on these results, we provide a near-optimal solution on α and β to the optimization problem of minimizing the error-rates. We also show that 3ϕ DASC-MF is less complex than DASC-MF, and a majority of the symbols transmitted during 3ϕ DASC-MF scheme are coordinated in energy. (See Sec. IV)

- 3) When $\Theta > \frac{L}{2}$, we propose a new countermeasure, referred to as the semi-coherent multiple access channel (SC-MAC) scheme. As a salient feature of this scheme, the helper does not decode the victim's symbols, instead, the victim and the helper transmit their symbols synchronously to the destination on the helper's frequency using an energy-splitting factor, $\varepsilon \in (0, 1)$, thereby, eliminating the need of an FD radio at the helper. For SC-MAC, we first derive a closed-form expression on the error-rates and then, formulate an optimization problem of finding near-optimal values on ε that minimizes the error-rates at the destination. (See Sec. V)
- 4) We also present extensive simulation results to show that using both the 3ϕ DASC-MF scheme and the SC-MAC scheme, the victim is able to reliably communicate with the destination while adhering to the deadline constraints. (See Sec. VI)
- 5) Finally, through various analytical and simulation results, we show that our schemes are covert when the adversary measures energy on the victim's and the helper's frequencies. (See Sec. VII)

C. Related Work

Due to the recent technological advancements in the FD radio architectures [4]–[10], FD radios have been studied from the viewpoints of mitigating adversaries [21]–[24] as well as aiding adversaries [25]–[27]. However, [15]–[19] have studied FD radios from both these viewpoints wherein an FD adversary is used to jam the network and an FD helper node is used to mitigate the FD jammer. When using an FD radio at the adversary, [15], [16], [18] presented *jam and measure* adversaries, that jams a frequency band and subsequently monitors it using FD cognitive radios [11]–[14] to detect countermeasures based on FH. Moreover, [15], [16] used countermeasure detectors based on energy measurement, while [18] used countermeasure detectors based on energy and correlation. In contrast, when using an FD radio at the helper node, [15], [16], [18] also proposed fast-forward FD relay based countermeasures to mitigate the *jam and measure* adversaries. Here, the authors leveraged on [21], which proposed a fast-forward FD relay that constructively forwards signals such that the network throughput and coverage is significantly enhanced. Along the similar lines of [15], [16], [18], authors in [17], [19] proposed fast-forward relaying based solutions to mitigate the *jam and measure* adversary, however in fast-fading channel conditions. We highlight that, when mitigating *jam and measure*

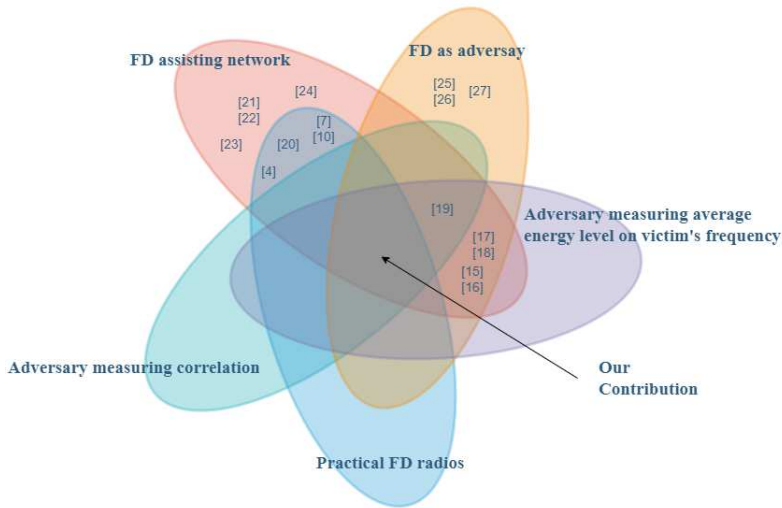


Fig. 1: Novelty of our work w.r.t. existing contributions.

adversaries, [15]–[19] assumed an optimistic scenario where the FD helper node instantaneously fast-forwards the victim’s information symbol to the destination. However, in practice since the processing delay for self-interference cancellation is directly proportional to the number of transmit/receive (or both) antennas at the helper node [20], the fast-forwarding process is not instantaneous. Thus, to bridge this gap, this work considers the practical limitations of delay-aware FD radios in facilitating reliable and low-latency communication of the victim’s symbols. As depicted in Fig. 1, the main novelty of this work is the use of delay-aware FD radios at the helper node, which has not been addressed in the literature hitherto.

II. SYSTEM MODEL

We consider a network model, where all the uplink frequencies to the destination are occupied by the legitimate nodes of the network. As a result, there are no vacant frequencies in the network. Let Alice and Charlie be two legitimate nodes of the network who communicate with the destination, Bob using orthogonal frequencies. Alice is a single-antenna transmitter which uses a frequency band centred around f_{AB} to communicate her low data-rate symbols with strict low-latency constraints

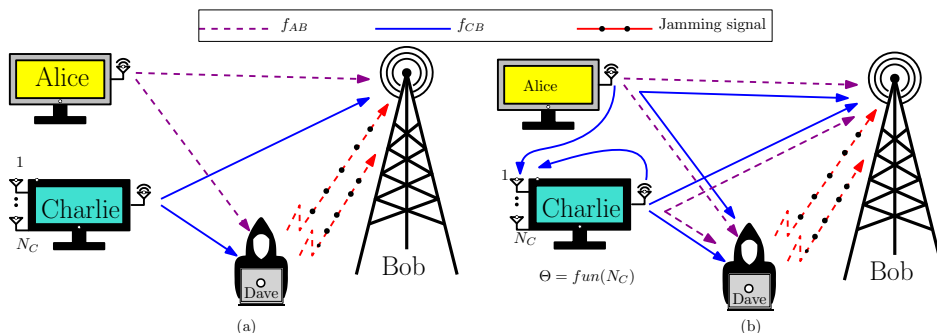


Fig. 2: (a) A network model depicting legitimate nodes, Alice and Charlie, and the reactive adversary, Dave. (b) System model for DASC-MF scheme, where Charlie takes Θ symbols to multiplex-and-forward Alice’s symbols to Bob.

(e.g., PUCCH in 5G [28]) to Bob. In contrast, Charlie uses a frequency band centred around f_{CB} to communicate his symbols to Bob. A salient feature of Charlie is that he is equipped with a full-duplex (FD) radio with N_C receive-antennas and a single transmit-antenna, thus, enabling him to implement FD communication on f_{CB} . Further, Charlie transmits symbols with arbitrary data-rate and relaxed latency constraints. An instantiation of the network is as shown in Fig. 2 (a).

In this network, we also assume the presence of a jammer, Dave. Unlike traditional jammers, Dave is an FD reactive jammer who intends to jam Alice's uplink symbols on f_{AB} [29] and monitors all the frequencies (including f_{AB}) for possible countermeasures by the legitimate nodes. In the context of this work, Dave uses an energy detector (ED) to measure the average energy level of all the frequencies in the network before and after jamming. Thus, if ED measures a significant fluctuation in the average energy level on any band, it raises the flag. This in turn forbids Alice from using traditional mitigation techniques, such as FH. Subsequently, a raised flag by ED compels Dave to jam other frequencies, thereby degrading the network's performance. Thus, in the next section, we propose a framework wherein Charlie assists Alice to reliably communicate her messages to Bob without getting detected by ED on any frequency band.

III. DELAY-AWARE SEMI-COHERENT MULTIPLEX-AND-FORWARD RELAYING SCHEME

As shown in Fig. 3, let Alice have a frame of L symbols to communicate with Bob within T seconds from the generation of the first symbol, where $T = L/W$, such that W is the bandwidth of communication. Since f_{AB} is jammed by Dave, Alice seeks help from Charlie. As part of the protocol, Alice broadcasts her symbols on f_{CB} . Then, Charlie, uses his FD radio to forward Alice's symbols to Bob on f_{CB} . Since Charlie is a legitimate node in the network, he also has symbols to communicate with Bob. Therefore, he decodes Alice's symbols, multiplexes her symbols to his symbols, and forwards them to Bob. However, the time taken by Charlie for this process depends on his receiver architecture. In particular, this *delay* is directly proportional to the time taken by him to cancel his self-interference (SI), which in turn is directly proportional to the number of receiving antennas, N_C . Therefore, we assume that Charlie requires a time duration equivalent to that of Θ symbols to decode, multiplex, and forward Alice's symbols, where Θ is governed by the SIC architecture of Charlie.

The top two frames in Fig. 3 show the symbols transmitted simultaneously by Alice and Charlie on f_{CB} . The received symbols at Bob, denoted by $r_{B,n}$ are captured by the bottom frame, where n denotes the symbol interval index for communication. Further, x_n denotes Alice's symbol, and y_n , for $1 \leq n \leq \Theta$ and t_n , for $\Theta + 1 \leq n \leq L + \Theta$ denote the unmultiplexed and multiplexed symbols transmitted by Charlie, respectively. Due to delay of Θ symbols, $r_{B,n}$ is a function of x_n and y_n , for $1 \leq n \leq \Theta$. In addition, $r_{B,n}$ is a function of $x_{n-\Theta}$, x_n , and y_n , for $\Theta + 1 \leq n \leq L$. Note that, since

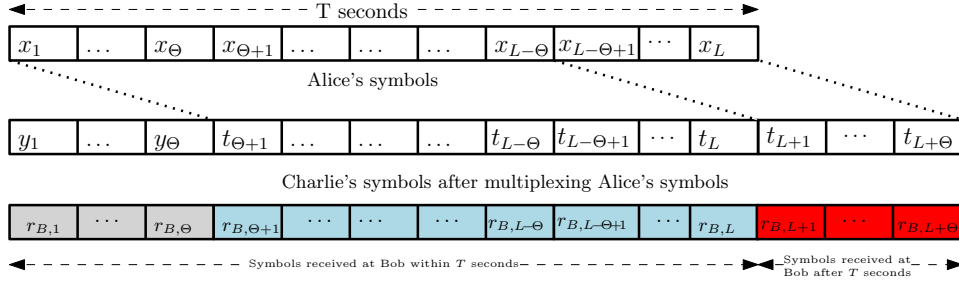


Fig. 3: Illustration of symbol transmission in DASC-MF scheme.

the multiplexed symbols, t_n , for $L + 1 \leq n \leq L + \Theta$ are received after the deadline of T seconds, Bob cannot use these symbols for decoding Alice's symbols due to latency constraints. Therefore, Bob only uses the first L symbols received on f_{CB} after implementing the proposed countermeasure to jointly decode Alice's and Charlie's symbols.¹

Although the above scheme ensures that Alice's symbols reach Bob within the deadline, Dave observes a significant drop in the energy level on f_{AB} , provided Alice uses her entire energy to communicate on f_{CB} . Therefore, to avoid getting detected by Dave, Alice and Charlie use $1 - \alpha$ and α fractions of their energies, respectively, to communicate their messages on f_{CB} , where $\alpha \in (0, 1)$ is the design parameter under consideration. Subsequently, Alice and Charlie also use α and $1 - \alpha$ fractions of their energies, respectively, to cooperatively transmit dummy OOK symbols on f_{AB} . The dummy OOK symbols are sampled from a pre-shared Gold sequence, thus, ensuring that the average energy level on f_{AB} is the same as it was before implementing the countermeasure. We highlight that the use of dummy OOK symbols also ensures that the symbols on f_{AB} and f_{CB} are uncorrelated. Fig. 2 (b) illustrates the transmission strategy by Alice and Charlie on both f_{AB} and f_{CB} .

Due to low-latency constraints, Alice avoids the use of pilots for assisting channel estimation on f_{CB} , as a result, the communication on the links Alice-to-Charlie and Alice-to-Bob are inherently non-coherent. Further, since Alice has low data-rate symbols, she uses OOK signalling scheme. In contrast, since f_{CB} is not under attack, Charlie uses a coherent signalling scheme. In particular, Charlie uses M -ary PSK to communicate with Bob. As a result, the proposed scheme is a combination of coherent and non-coherent communication under a multiple access channel setup. Further, since this scheme takes into account the delay in processing Alice's symbols at Charlie, we refer to the proposed scheme as Delay-Aware Semi-Coherent Multiplex-and-Forward (DASC-MF) scheme.

In the next section, we discuss the signal model of DASC-MF scheme on f_{CB} . A detailed description of communication on f_{AB} and the analysis on the energy detectors will be discussed in Sec. VII.

¹During implementation, Charlie may decide not to multiplex after the L -th symbol interval since Alice's symbols are no longer used for decoding from $r_{B,n}$ for $n > L$

A. Signal Model

In the DASC-MF scheme, Alice transmits $x_n \in \{0, 1\}$ scaled by $\sqrt{1-\alpha}$ throughout the entire frame. Since Charlie is equipped with an FD radio with N_C receive-antennas, the $N_C \times 1$ received vector at Charlie is given by

$$r_C \mathbf{r}_{C,n} = \sqrt{1-\alpha} \mathbf{h}_{AC,n} x_n + \mathbf{h}_{CC,n} + \mathbf{w}_{C,n}, \quad 1 \leq n \leq L, \quad (1)$$

where $\mathbf{h}_{AC,n} \sim \mathcal{CN}(\mathbf{0}_{N_C}, \sigma_{AC}^2 \mathbf{I}_{N_C})$, $\mathbf{h}_{CC,n} \sim \mathcal{CN}(\mathbf{0}_{N_C}, \lambda \frac{1+\alpha}{2} \mathbf{I}_{N_C})$, and $\mathbf{w}_{C,n} \sim \mathcal{CN}(\mathbf{0}_{N_C}, N_o \mathbf{I}_{N_C})$ are the $N_C \times 1$ vectors of fading channel coefficients of Alice-to-Charlie's link, residual SI of Charlie's FD radio, and the Additive White Gaussian Noise (AWGN) at Charlie, respectively, such that $\mathbf{0}_{N_C}$ is the $N_C \times 1$ vector of zeros and \mathbf{I}_{N_C} is the $N_C \times N_C$ Identity matrix. Further, $\lambda \in [0, 1]$ denotes the level of residual SI after the active and passive cancellations at Charlie. Finally, $N_o = \text{SNR}^{-1}$ is the variance of each element of the AWGN vector.

Charlie first uses non-coherent energy detection to decode x_n as \hat{x}_n using the received vector, $\mathbf{r}_{C,n}$ and then multiplexes the decoded symbol, \hat{x}_n to his symbol. However, due to the use of multiple receive-antennas, Charlie introduces a delay equivalent to Θ symbols to decode and multiplex \hat{x}_n to his current symbol after SIC. Therefore, a symbol received at Charlie from Alice during the n^{th} symbol interval is multiplexed and forwarded to Bob during the $(n+\Theta)^{\text{th}}$ symbol interval. As a result, for all $1 \leq n \leq \Theta$, if $y_n \in \mathcal{S}_C$ denotes the original PSK symbol of Charlie to be transmitted at n^{th} symbol interval, such that $\mathcal{S}_C = \left\{ e^{j\frac{\pi}{M}(2m+1)} \mid m = 0, \dots, M-1 \right\}$, Charlie transmits $\sqrt{\alpha} y_n$. Subsequently, for all $n \geq \Theta + 1$, Charlie transmits the multiplexed symbol, t_n , such that

$$t_n = \begin{cases} y_n, & \text{if } \hat{x}_{n-\Theta} = 0, \\ \sqrt{\alpha} e^{j\frac{\pi}{M}} y_n, & \text{if } \hat{x}_{n-\Theta} = 1. \end{cases} \quad (2a)$$

$$t_n = \begin{cases} y_n, & \text{if } \hat{x}_{n-\Theta} = 0, \\ \sqrt{\alpha} e^{j\frac{\pi}{M}} y_n, & \text{if } \hat{x}_{n-\Theta} = 1. \end{cases} \quad (2b)$$

With this transmission strategy, Bob observes a multiple access channel on f_{CB} from Alice and Charlie. We note that Alice's symbol transmitted during the n^{th} symbol interval is observed at Bob during n^{th} time symbol on Alice-to-Bob link on $r_{B,n}$ and is again observed as multiplexed symbol from Charlie at $(n+\Theta)^{\text{th}}$ time symbol on Charlie-to-Bob link on $r_{B,n+\Theta}$, thus, introducing correlation between $r_{B,n}$ and $r_{B,n+\Theta}$. Overall, the received symbol at Bob during n^{th} symbol interval is given as

$$r_{B,n} = \begin{cases} \sqrt{1-\alpha} h_{AB,n} x_n + \sqrt{\alpha} h_{CB,n} y_n + w_{B,n}, & \text{if } 1 \leq n \leq \Theta, \\ \sqrt{1-\alpha} h_{AB,n} x_n + h_{CB,n} t_n + w_{B,n}, & \text{if } \Theta + 1 \leq n \leq L, \end{cases} \quad (3a)$$

$$r_{B,n} = \begin{cases} \sqrt{1-\alpha} h_{AB,n} x_n + \sqrt{\alpha} h_{CB,n} y_n + w_{B,n}, & \text{if } 1 \leq n \leq \Theta, \\ \sqrt{1-\alpha} h_{AB,n} x_n + h_{CB,n} t_n + w_{B,n}, & \text{if } \Theta + 1 \leq n \leq L, \end{cases} \quad (3b)$$

where $h_{AB,n} \sim \mathcal{CN}(0, \sigma_{AB}^2)$ and $h_{CB,n} \sim \mathcal{CN}(0, \sigma_{CB}^2)$ are the channel coefficients of Alice-to-Bob and Charlie-to-Bob links, respectively. Further, $w_{B,n} \sim \mathcal{CN}(0, N_o)$ is the AWGN at Bob during the n^{th} symbol interval. For the decoding process, we assume that Bob has the knowledge of $h_{CB,n}$. Further, since Charlie is in the vicinity of Alice, we assume $\sigma_{AC}^2 > \sigma_{AB}^2$, thus achieving a higher SNR on

Alice-to-Charlie link as compared to Alice-to-Bob link. We also assume that all channels and noise realizations are statistically independent. Finally, for error analysis in the rest of the paper, we use $\sigma_{AB}^2 = \sigma_{CB}^2 = 1$.

B. Error Analysis at Bob

Since Charlie decodes and multiplexes Alice's symbols to Bob, in this section, we first characterise the error introduced by Charlie in decoding Alice's symbols. We then compute the joint error-rates at Bob in decoding Alice's and Charlie's symbols.

Based on (1), the maximum likelihood (ML) decoder for detection of Alice's symbols at Charlie is

$$rCl\hat{x}_n = \arg \max_{i \in \{0,1\}} g(\mathbf{r}_{C,n}|x_n = i) = \arg \min_{i \in \{0,1\}} N_C \ln(\pi\Omega_i) + \frac{\mathbf{r}_{C,n}^H \mathbf{r}_{C,n}}{\Omega_i}, \quad (4)$$

where $g(\mathbf{r}_{C,n}|x_n)$ is the probability density function (PDF) of $\mathbf{r}_{C,n}$ conditioned on x_n and $\Omega_i = \sigma_{AC}^2(1 - \alpha)i + \lambda \frac{(1+\alpha)}{2} + N_o$. Based on (4), the threshold for energy detection is given by $\tau = N_C \frac{\Omega_0 \Omega_1}{\Omega_0 - \Omega_1} \ln\left(\frac{\Omega_0}{\Omega_1}\right)$. Finally, using τ , it is straightforward to prove the next theorem that presents the probability of error at Charlie in decoding Alice's symbols.

Theorem 1. *If $\Phi_{\bar{i}\bar{i}}$ denotes the probability of decoding symbol i as \bar{i} , for $i, \bar{i} = \{0, 1\}$, then $\Phi_{01} = \frac{\Gamma(N_C, \frac{\tau}{\Omega_0})}{\Gamma(N_C)}$ and $\Phi_{10} = \frac{\gamma(N_C, \frac{\tau}{\Omega_1})}{\Gamma(N_C)}$, where $\Gamma(\cdot, \cdot)$ and $\gamma(\cdot, \cdot)$ denote the lower and upper incomplete gamma functions, respectively, and $\Gamma(\cdot)$ denotes the complete gamma function.*

From Theorem 1, we immediately observe the following two remarks.

Remark 1. *The terms Φ_{01} and Φ_{10} are increasing functions of α for a given N_C , SNR, and λ .*

Remark 2. *The terms Φ_{01} and Φ_{10} are decreasing functions of N_C , for a given α , SNR, and λ .*

Based on (3a) and (3b), the joint maximum a posteriori (MAP) decoder for DASC-MF scheme is

$$rCl\hat{i}, \hat{j}, \hat{k}, \hat{l} = \arg \max_{i,j,k,l} g_B\left(r_{B,n}, r_{B,n-\Theta}|x_n = i, x_{n-\Theta} = j, y_n = e^{t\frac{\pi}{M}(2l+1)}, y_{n-\Theta} = e^{t\frac{\pi}{M}(2k+1)}, h_{CB,n}, h_{CB,n-\Theta}\right), \quad (5)$$

where $i, j \in \{0, 1\}$, $k, l \in \{0, M - 1\}$ and $g_B(\cdot)$ is the joint PDF of $r_{B,n}$ and $r_{B,n-\Theta}$ conditioned on x_n and y_n for $1 \leq n \leq \Theta$ and $x_n, x_{n-\Theta}, y_{n-\Theta}$, and y_n , for $\Theta + 1 \leq n \leq L$.

Towards decoding Alice's and Charlie's symbols, the implementation of the decoder in (5) is complex due to the correlation between the symbols received Θ symbols apart. In particular, the complexity of the proposed decoder is $\mathcal{O}(4M^2)$ as Bob has to jointly decode two OOK and two PSK symbols. Further, we note that, at any instant the symbols transmitted by Alice and Charlie are uncoordinated in their energies. For instance, when Alice transmits bit-0, Alice and Charlie contribute zero and α energies, respectively. Thus, the resultant sum energy on f_{CB} is α . As a result, Dave's ED that is monitoring f_{CB} may observe a dip in the average energy level on f_{CB} . Therefore,

to circumvent the above problems, in the next section, we propose a variation of DASC-MF scheme, such that the new scheme is amenable to lower-decoding complexity at Bob. Further, the new scheme also ensures that despite uncoordinated transmission from Alice and Charlie, the duration for which Dave's ED observes a dip in the average energy level on f_{CB} is small.

IV. 3ϕ DELAY TOLERANT SEMI-COHERENT MULTIPLEX-AND-FORWARD RELAYING SCHEME

From the discussions in the previous section, we note that Alice's information symbol, x_n , $1 \leq n \leq L - \Theta$ is observed twice at Bob during the interval of T seconds: once during the symbol interval $1 \leq n \leq L - \Theta$ on the Alice-to-Bob link of the MAC and again after Θ symbols as t_n , for $\Theta + 1 \leq n \leq L$ on the Charlie-to-Bob link of the MAC. Therefore, if Bob discards Alice's symbols on Alice-to-Bob link of the MAC for $1 \leq n \leq L - \Theta$ and treat these symbols as interference, he can still recover these symbols using the multiplexed symbols t_n , $\Theta + 1 \leq n \leq L$. Furthermore, if the interference caused from Alice's symbols on the symbol intervals $1 \leq n \leq L - \Theta$ are somehow suppressed, then the correlation between $r_{B,n}$ and $r_{B,n+\Theta}$ can be minimized, thereby ensuring that Charlie's symbols on $r_{B,n}$ are decoded independent of Charlie's multiplexed symbols on the other symbol intervals. Subsequently this would facilitate reduced decoding complexity at Bob. To facilitate interference suppression, we propose a method of choosing α for the symbol intervals $1 \leq n \leq L - \Theta$, such that Charlie would continue to reliably recover Alice's symbols for multiplexing process. We note that, since the Alice-to-Bob link of the MAC is non-coherent, Alice contributes $1 - \alpha$ and zero energies on this link for $x_n = 1$ and $x_n = 0$, respectively. As a result, the variance of the effective noise at Bob is utmost $N_o + 1 - \alpha$ and N_o for $x_n = 1$ and $x_n = 0$, respectively. Since $N_o + 1 - \alpha$ is a decreasing function of α , if we increase α close to 1, we can suppress the interference on Alice-to-Bob link of the MAC, when $x_n = 1$ is sent from Alice. In particular, if $1 - \alpha = \Delta N_o$, such that $0 < \Delta \ll 1$, where Δ is the design parameter, then, $N_o + 1 - \alpha = N_o(1 + \Delta) \approx N_o$. However, we must note that, when α is close to 1, Charlie requires a large N_C to reliably decode Alice's symbols (Remark 1). Therefore, if we indefinitely reduce Δ to a very small value to increase α close to 1, N_C increases which in turn increases the latency at Charlie. Thus, in our proposed scheme, interference suppression at Bob comes at a cost of large N_C .

From the above discussion, the transmission scheme for the symbol intervals, $1 \leq n \leq L$ at Alice and Charlie can be divided into three phases. During Phase-I, $1 \leq n \leq \Theta$, Alice and Charlie transmit their symbols scaled by $1 - \alpha$ and α fractions of their energies, respectively. Subsequently, during Phase-II, $\Theta + 1 \leq n \leq L - \Theta$, Alice continues to transmit her symbols scaled by $1 - \alpha$ fraction of her energy, however, Charlie scales the multiplexed symbol by α fraction of his energy as given in (2a) - (2b). Further, due to processing delay of Θ symbols at Charlie, the multiplexed symbols

corresponding to x_n , $L - \Theta + 1 \leq n \leq L$, reach Bob after the deadline i.e., after T seconds. Therefore, these symbols cannot be decoded using the multiplexed symbols and instead must be decoded using the symbols on Alice-to-Bob link of the MAC. Thus, for $L - \Theta + 1 \leq n \leq L$, Bob must jointly decode three symbols, i.e., Alice's current symbol, x_n , Charlie's current symbol, y_n , and multiplexed Alice's symbol, $x_{n-\Theta}$. Since these symbols are transmitted via combination of coherent and non-coherent modulation schemes, Bob needs distinguishable energy levels for detection when $x_n = 0$ and $x_n = 1$ is sent. As a consequence, for $L - \Theta + 1 \leq n \leq L$, we cannot use $\alpha = 1 - \Delta N_o$ and instead use a different energy-splitting factor, $\beta \in (0, 1)$. Therefore, we refer to the symbol intervals $L - \Theta + 1 \leq n \leq L$ as Phase-III, wherein, Alice and Charlie transmit their symbols scaled by $1 - \beta$ and β fraction of their energies, respectively. Here, Charlie only rotates his PSK symbol by $e^{j\frac{\pi}{M}}$ when he decodes symbol 1 from Alice. It is evident from the discussions that the maximum delay tolerated by the proposed 3ϕ DASC-MF scheme is $\frac{L}{2}$, i.e., $\Theta \leq \frac{L}{2}$. This is because, for $\Theta > \frac{L}{2}$, only a fraction of Alice's symbols are recoverable using Charlie's multiplexed symbols and a majority of the multiplexed symbols are received after the deadline, thus, violating the deadline constraint.

Overall, the symbols received at Bob during each phase are tabulated in Table I. Further, in Fig. 4, the top two frames depict the symbols transmitted by Alice and Charlie when using the 3ϕ DASC-MF scheme. The bottom frame depicts the corresponding symbols received at Bob during each phase. Furthermore, assuming Charlie transmits symbols using 4-PSK signalling, the constellation diagrams jointly contributed by Alice and Charlie during each phase at Bob are shown in Fig. 5.

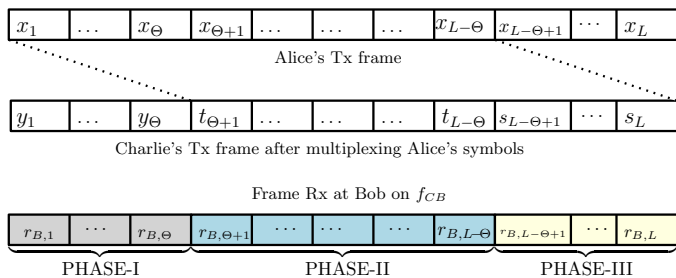


Fig. 4: Frame model for the 3ϕ DASC-MF scheme.

TABLE I: SYMBOLS TRANSMITTED IN EACH PHASE

	Alice-to-Bob link	Charlie-to-Bob link
Phase-I	$\sqrt{1 - \alpha}x_n$	$\sqrt{\alpha}y_n$
Phase-II	$\sqrt{1 - \alpha}x_n$	$t_n = \begin{cases} y_n & \text{if } \hat{x}_{n-\Theta} = 0, \\ \sqrt{\alpha}e^{j\frac{\pi}{M}}y_n & \text{if } \hat{x}_{n-\Theta} = 1. \end{cases}$
Phase-III	$\sqrt{1 - \beta}x_n$	$s_n = \begin{cases} \sqrt{\beta}y_n & \text{if } \hat{x}_{n-\Theta} = 0, \\ \sqrt{\beta}e^{j\frac{\pi}{M}}y_n & \text{if } \hat{x}_{n-\Theta} = 1. \end{cases}$

From the above discussions, it is clear that, the decoding complexities during Phase-I, Phase-II and Phase-III are $\mathcal{O}(M)$, $\mathcal{O}(2M)$, and $\mathcal{O}(4M)$, respectively. Hence, unlike DASC-MF scheme, the worst-case complexity of 3ϕ DASC-MF is linear in M . Further, since α is close to 1, for $1 \leq n \leq L - \Theta$, the energy level on f_{CB} is solely controlled by Charlie and only the last Θ symbols out of the L symbols received at Bob are uncoordinated in energy. In particular, in 3ϕ DASC-MF scheme, $\frac{\Theta}{L}$ fraction of symbols are uncoordinated in energy, whereas, in traditional DASC-MF scheme, the entire frame of L symbols are uncoordinated in energy. Hence, 3ϕ DASC-MF scheme helps reduce the decoding complexity and reduce the fraction of symbols over which the energy is uncoordinated.

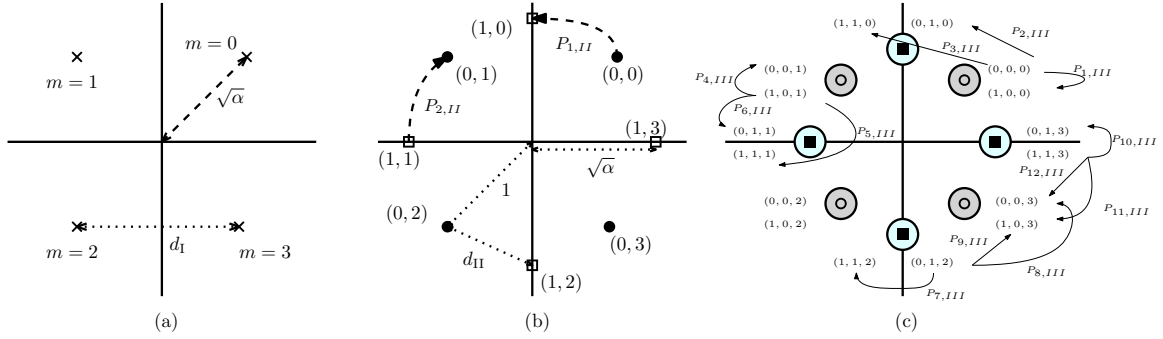


Fig. 5: Constellation diagram depicting the symbols jointly contributed by Alice and Charlie during each phase in the 3ϕ DASC-MF as a function of x_n , $x_{n-\Theta}$, and y_n : (a) Phase-I (b) Phase-II (c) Phase-III.

Towards characterising the error performance of the 3ϕ DASC-MF scheme, if $P_{e,3\phi}$ denotes the average probability of error across all the three phases, then

$$rClP_{e,3\phi} = \frac{\Theta}{L}P_{I,avg} + \frac{(L-2\Theta)}{L}P_{II,avg} + \frac{\Theta}{L}P_{III,avg}, \quad (6)$$

where $P_{I,avg}$ denotes the average probability of error in decoding y_n , $1 \leq n \leq \Theta$, during Phase-I, $P_{II,avg}$ denotes the average probability of error in jointly decoding y_n and $x_{n-\Theta}$, $\Theta+1 \leq n \leq L-\Theta$, during Phase-II, and $P_{III,avg}$ denotes the average probability of error in jointly decoding x_n , y_n , $x_{n-\Theta}$, $L-\Theta+1 \leq n \leq L$, during Phase-III. All the error terms in (6) are averaged over $h_{CB,n}$, $1 \leq n \leq L$. Note that, here, $P_{I,avg}$ is a function of α , $P_{II,avg}$ is a function of N_C and α , and $P_{III,avg}$ is a function of N_C and β . Since $\alpha = 1 - \Delta N_o$ is fixed for a given choice of Δ and SNR, the parameters of interest are N_C and β . Therefore, in (7) we formulate an optimization problem to compute the optimal values of N_C and β for a given L , Δ and SNR.

$$rClN_C^*, \beta^* = \arg \min_{N_C, \beta} P_{e,3\phi}; \quad \text{s.t.: } N_C > 1, 0 < \beta < 1. \quad (7)$$

In the subsequent sections, we discuss the signal model for all the three phases in detail and compute $P_{I,avg}$, $P_{II,avg}$, and $P_{III,avg}$, so as to obtain $P_{e,3\phi}$.

A. Signal Model and Error Analysis of Phase-I

During Phase-I, Bob receives the first Θ symbols of Alice on Alice-to-Bob link of the MAC scaled by the factor $\sqrt{1-\alpha}$ and the unmultiplexed symbols of Charlie scaled by the factor $\sqrt{\alpha}$ on Charlie-to-Bob link of the MAC. However, according to the protocol of 3ϕ DASC-MF scheme, Bob treats the incoming symbols from Alice on the Alice-to-Bob link of the MAC as interference. Thus, the n^{th} baseband symbol received at Bob during Phase-I is given as $r_{B,n} = h_{CB,n}\sqrt{\alpha}y_n + \tilde{w}_{B,n}$, for $1 \leq n \leq \Theta$, where $\tilde{w}_{B,n} = \sqrt{1-\alpha}h_{AB,n}x_n + w_{B,n}$ denotes the effective noise at Bob, such that $N_{o\alpha} = N_o + 1 - \alpha$ is its worst case effective variance. Given that α is close to 1, we assume that $\tilde{w}_{B,n} \sim \mathcal{CN}(0, N_{o\alpha})$. For

4-PSK signalling scheme, the constellation diagram during Phase-I at Bob is as shown in Fig. 5 (a), where m denotes the index of the PSK symbol transmitted by Charlie. Owing to the Gaussian statistics of $\tilde{w}_{B,n}$ and $h_{CB,n}$, $r_{B,n}|y_n, h_{CB,n} \sim \mathcal{CN}(\sqrt{\alpha}h_{CB,n}y_n, N_{o\alpha})$. Since the symbols received at Bob during Phase-I only contains Charlie's symbols, based on $r_{B,n}$, the Maximum A Posteriori (MAP) decoder for Phase-I is

$$rCl\hat{m} = \arg \max_m g_I \left(r_{B,n}|y_n = e^{t\frac{\pi}{M}(2m+1)}, h_{CB,n} \right), \quad (8)$$

where $m \in \{0, \dots, M-1\}$ and $g_I(\cdot)$ is the PDF of $r_{B,n}$ conditioned on $h_{CB,n}$ and y_n . Further, \hat{m} denotes the decoded PSK index. Using (8), in the following theorem, we characterise the average probability of error over all the realizations of $h_{CB,n}$, denoted by $P_{1,avg}$.

Theorem 2. *At high SNR, a union bound on the probability of error during Phase-I is approximated as $2Q\left(\frac{h_{CB,n}|d_1}{\sqrt{2N_{o\alpha}}}\right)$, where $Q(\cdot)$ denotes the Q-function. Further, we first use Chernoff bound to upper bound the error expression and then average it over all the realizations of $h_{CB,n}$ to obtain \mathcal{P}_1 , such that $\mathcal{P}_I = \frac{4N_{o\alpha}}{4N_{o\alpha} + d_1^2}$. [30]*

B. Signal Model and Error Analysis of Phase-II

During Phase-II, Alice continues to transmit her OOK symbol, x_n , with $1 - \alpha$ fraction of her energy and Charlie transmits the multiplexed symbol t_n , which is a function of y_n and $x_{n-\Theta}$. Thus, Bob receives Alice's symbols on the Alice-to-Bob link of the MAC and Charlie's multiplexed symbols on the Charlie-to-Bob link of the MAC. However, he considers Alice's symbols as interference and jointly decodes y_n and $x_{n-\Theta}$. The n^{th} baseband symbol received during Phase-II at Bob is given as $r_{B,n} = h_{CB,n}t_n + \tilde{w}_{B,n}$, for $\Theta + 1 \leq n \leq L - \Theta$, where t_n is as given in Table I and $\tilde{w}_{B,n}$ is the effective noise at Bob. Fig. 5 (b) depicts the constellation received at Bob during Phase-II. If Alice and Charlie choose to transmit $x_{n-\Theta} = j$ and $y_n = e^{t\frac{\pi}{M}(2m+1)}$, then the transmit pair is denoted by (j, m) . It can be observed that for 4-PSK used by Charlie, Bob can receive one out of the 8 symbols. In general, when Charlie uses M -PSK constellation, Bob receives one out of the $2M$ constellation points. Therefore, the distribution of $r_{B,n}$ conditioned on $x_{n-\Theta}$, y_n , and $h_{CB,n}$ is

$$\begin{cases} \mathcal{CN}(h_{CB,n}y_n, N_{o\alpha}) & \text{if } x_{n-\Theta} = 0 \text{ and } \hat{x}_{n-\Theta} = x_{n-\Theta} \text{ or } x_{n-\Theta} = 1 \text{ and } \hat{x}_{n-\Theta} \neq x_{n-\Theta}, \quad (9a) \\ \mathcal{CN}(\sqrt{\alpha}h_{CB,n}e^{t\frac{\pi}{M}(2m+1)}y_n, N_{o\alpha}) & \text{if } x_{n-\Theta} = 0 \text{ and } \hat{x}_{n-\Theta} \neq x_{n-\Theta} \text{ or } x_{n-\Theta} = 1 \text{ and } \hat{x}_{n-\Theta} = x_{n-\Theta}. \quad (9b) \end{cases}$$

Using (9a) – (9b), the joint MAP decoder for Phase-II is given by

$$rCl\hat{j}, \hat{m} = \arg \max_{j,m} g_{II} \left(r_{B,n}|x_{n-\Theta} = j, y_n = e^{t\frac{\pi}{M}(2m+1)}, h_{CB,n} \right), \quad (10)$$

where $j \in \{0, 1\}$ and $m \in \{0, \dots, M-1\}$. Further, $g_{II}(\cdot)$ is the conditional PDF of $r_{B,n}$ conditioned on $x_{n-\Theta}$, y_n , and $h_{CB,n}$. Note that due to errors introduced by Charlie in decoding Alice's symbols, the

distribution of $g_{II}(\cdot)$ is a Gaussian mixture. In particular, the distribution of $g_{II}(\cdot)$ is a convex combination of $g_{II}(r_{B,n}|y_n, h_{CB,n}, x_{n-\theta} = \hat{x}_{n-\theta})$ and $g_{II}(r_{B,n}|e^{t\frac{\pi}{M}}y_n, h_{CB,n}, x_{n-\theta} \neq \hat{x}_{n-\theta})$, when $x_{n-\theta} = 0$ and $x_{n-\theta} = 1$. The distribution of $g_{II}(\cdot)$ for different realizations of $x_{n-\theta}$ is as given in (11).

$$g_{II}(r_{B,n}|x_{n-\theta} = j, y_n, h_{CB,n}) = \Phi_{jj}g_{II}(r_{B,n}|y_n, h_{CB,n}, x_{n-\theta} = \hat{x}_{n-\theta}) + \Phi_{j\bar{j}}g_{II}(r_{B,n}|e^{t\frac{\pi}{M}}y_n, h_{CB,n}, x_{n-\theta} \neq \hat{x}_{n-\theta}), \quad (11)$$

where \bar{j} is the complement of j and $\Phi_{00} = 1 - \Phi_{01}$ and $\Phi_{11} = 1 - \Phi_{10}$ are the probabilities of correct detection of bit-0 and bit-1 at Charlie, respectively. Further, $g_{II}(r_{B,n}|e^{t\frac{\pi}{M}}y_n, h_{CB,n}, x_{n-\theta} \neq \hat{x}_{n-\theta})$ is the conditional PDF of the symbol received at Bob when Charlie makes an error in decoding Alice's symbol. Since solving the error-performance of the joint MAP decoder using the Gaussian mixtures is non-trivial, we propose an approximation on (10), where we only consider the dominant term in (11) for error computation, for each realization of j . Along the similar lines of [16], we observe that Φ_{00} is dominant over Φ_{01} when $x_{n-\theta} = 0$ and Φ_{11} is dominant over Φ_{10} , when $x_{n-\theta} = 1$. Therefore, we approximate the joint MAP decoder in (10) by a Joint Dominant Decoder (JDD), by retaining the first term in the RHS of (11). The expression of JDD is given as

$$rCl\hat{j}, \hat{m} = \arg \max_{j,m} \tilde{g}_{II}(r_{B,n}|x_{n-\theta} = j, y_n = e^{t\frac{\pi}{M}(2m+1)}, h_{CB,n}), \quad (12)$$

where $j \in \{0, 1\}$ and $m \in \{0, \dots, M-1\}$. Further, $\tilde{g}_{II}(\cdot)$ is an approximation on $g_{II}(\cdot)$ when considering the first term in the RHS of (11). In the next theorem, we derive a union bound on the probability of error in jointly decoding Alice's and Charlie's symbols during Phase-II.

Theorem 3. *At high SNR, the probability of error for Phase-II, denoted by $P_{e,II}$, is upper bounded by $\Phi_{00}P_{1,II} + \Phi_{01}P_{\bar{1},II} + \Phi_{11}P_{2,II} + \Phi_{10}P_{\bar{2},II}$, where $P_{1,II} = P_{2,II}$ and $P_{\bar{1},II} = P_{\bar{2},II} = 1 - P_{1,II}$, such that $P_{1,II} \approx Q\left(\frac{h_{CB,n}|d_{II}}{\sqrt{2N_{\alpha}}}\right)$. Here, $d_{II} = \sqrt{1 + \alpha - 2\sqrt{\alpha} \cos\left(\frac{\pi}{M}\right)}$ denotes the minimum Euclidean distance between the constellation points transmitted by Charlie during Phase-II.*

Proof. Let a transmit pair corresponding to $x_{n-\theta}$ and y_n is denoted by (j, m) , such that y_n denotes the PSK symbol transmitted by Charlie corresponding to the index m . Let $\nabla_{(j,m) \rightarrow (j',m')}$ be the event $(j', m') \neq (j, m)$, then a pair (j, m) is incorrectly decoded as (j', m') if

$$rCl\nabla_{(j,m) \rightarrow (j',m')} \triangleq \frac{\tilde{g}_{II}(r_{B,n}|x_{n-\theta} = j, y_n = e^{t\frac{\pi}{M}(2m+1)}, h_{CB,n})}{\tilde{g}_{II}(r_{B,n}|x_{n-\theta} = j', y_n = e^{t\frac{\pi}{M}(2m'+1)}, h_{CB,n})} \leq 1.$$

Therefore, the probabilities of decoding a pair $(0, m)$ as (j', m') and $(1, m)$ as (j', m') at Bob is

$$rCl\Pr((0, m) \rightarrow (j', m')) = \Phi_{00}\Pr(\nabla_{(0,m) \rightarrow (j',m')} \leq 1 | \hat{x}_{n-\theta} = x_{n-\theta}) + \Phi_{01}\Pr(\nabla_{(0,m) \rightarrow (j',m')} \leq 1 | \hat{x}_{n-\theta} \neq x_{n-\theta}) \quad (3)$$

$$\Pr((1, m) \rightarrow (j', m')) = \Phi_{11}\Pr(\nabla_{(1,m) \rightarrow (j',m')} \leq 1 | \hat{x}_{n-\theta} = x_{n-\theta}) + \Phi_{10}\Pr(\nabla_{(1,m) \rightarrow (j',m')} \leq 1 | \hat{x}_{n-\theta} \neq x_{n-\theta}) \quad (4)$$

Combining (13) and (14), the probability of error in decoding a transmit pair (j, m) as (j', m') is

$$rClPr((j, m) \rightarrow (j', m')) = \Phi_{jj} \Pr(\nabla_{(j,m) \rightarrow (j',m')} \leq 1 | \hat{x}_{n-\Theta} = x_{n-\Theta}) + \Phi_{\bar{j}\bar{j}} \Pr(\nabla_{(j,m) \rightarrow (j',m')} \leq 1 | \hat{x}_{n-\Theta} \neq x_{n-\Theta}). \quad (15)$$

Therefore, if the overall probability of error in decoding a transmit pair (j, m) is denoted by $\Pr((\hat{j}, \hat{m}) \neq (j, m))$, then an upper bound on the overall expression is

$$rClPr((\hat{j}, \hat{m}) \neq (j, m)) \leq \sum_{\substack{j'=0 \\ (j',m') \neq (j,m)}}^1 \sum_{m'=0}^{M-1} \Pr((j, m) \rightarrow (j', m')). \quad (16)$$

As discussed earlier, Bob receives one out of the $2M$ -PSK symbols corresponding to the M -PSK constellation used by Charlie. Finally, if $P_{e,II}$ denotes the average probability of error over $2M$ symbols, then using (13) - (16), it is straightforward to compute an upper bound on $P_{e,II}$ as $P_{e,II} \leq \frac{1}{2M} \sum_{j=0}^1 \sum_{m=0}^{M-1} M \Pr((\hat{j}, \hat{m}) \neq (j, m)) \approx \Phi_{00}P_{1,II} + \Phi_{01}P_{\bar{1},II} + \Phi_{11}P_{2,II} + \Phi_{10}P_{\bar{2},II}$. Here, we only considered the nearest-neighbours at high SNR to approximate the upper bound. The pairwise probability terms in $P_{e,II}$ are depicted in Fig. 5 (b). When evaluating the various error terms in the upper bound, we observe that $P_{1,II} = P_{2,II}$ and $P_{\bar{1},II} = P_{\bar{2},II} = 1 - P_{1,II}$, such that $P_{1,II} \approx Q\left(\frac{|h_{CB,n}|d_{II}}{\sqrt{2N_{o\alpha}}}\right)$. Here, $d_{II} = \sqrt{1 + \alpha - 2\sqrt{\alpha} \cos\left(\frac{\pi}{M}\right)}$ denotes the minimum Euclidean distance between the constellation points transmitted by Charlie during Phase-II. \square

Corollary 1. *If $P_{II,avg} = \mathbb{E}_{h_{CB,n}}[P_{e,II}]$ denotes the average probability of error over all the realizations of $h_{CB,n}$, then, using the Chernoff bound $P_{II,avg} \leq \mathcal{P}_{II} \triangleq \frac{2N_{o\alpha}}{4N_{o\alpha} + d_{II}^2} (\Phi_{00} + \Phi_{11}) + (\Phi_{01} + \Phi_{10})$, where we have used $P_{\bar{1},II} \leq 1$, $P_{\bar{2},II} \leq 1$ in the upper bound given in Theorem 3.*

C. Signal Model and Error Analysis of Phase-III

During Phase-III, Bob observes the symbols on both the links, i.e., the Alice-to-Bob link of the MAC and the Charlie-to-Bob of the MAC to decode x_n , y_n , and $x_{n-\Theta}$, for $L - \Theta + 1 \leq n \leq L$. Unlike Phase-I and Phase-II, Alice and Charlie use the energy-splitting factor, $\beta \in (0, 1)$ to transmit their respective symbols. In particular, Charlie scales his PSK symbols with $\sqrt{\beta}$, irrespective of $\hat{x}_{n-\Theta} = 0$ or $\hat{x}_{n-\Theta} = 1$. Further, Alice transmits her OOK symbols with $1 - \beta$ fraction of her energy. With this modification, the n^{th} baseband symbol received at Bob during Phase-III is given as

$$rClr_{B,n} = h_{AB,n}\sqrt{1 - \beta}x_n + h_{CB,n}\sqrt{\beta}s_n + w_{B,n}, \quad L - \Theta + 1 \leq n \leq L, \quad (17)$$

where s_n is defined in Table I and $w_{B,n} \sim \mathcal{CN}(0, N_o)$ is the AWGN at Bob. Owing to the non-coherent nature of Alice-to-Bob link of the MAC, the variance of the effective noise is $N_o + 1 - \beta$ and N_o , when $x_n = 1$ and $x_n = 0$, respectively. Fig. 5 (c) depicts the received constellation symbols at Bob during Phase-III, when Charlie uses 4-PSK signalling. If Alice's current symbol, $x_n = i$, Alice's multiplexed

symbol, $x_{n-\Theta} = j$, and Charlie's current symbol, $y_n = e^{j\frac{\pi}{M}(2m+1)}$, then a transmit triplet is denoted by (i, j, m) . The variance of the effective noise corresponding to $i = 0$ is N_o (small disk and solid squares), whereas, the variance of the effective noise corresponding to $i = 1$ is $N_o + 1 - \beta$ (blue and grey disks). We highlight that, Bob receives one out of the 16-PSK symbols corresponding to 4-PSK used by Charlie. In general, when Charlie uses M -PSK constellation, Bob is likely to receive one out of the $4M$ -PSK symbols, out of which, $2M$ -PSK symbols are received with variance N_o and the rest $2M$ -PSK symbols are received with variance $N_o + 1 - \beta$. The distribution of $r_{B,n}$ as a function of x_n , $x_{n-\Theta}$, y_n , and $h_{CB,n}$ is $r_{B,n}|x_n, x_{n-\Theta}, y_n, h_{CB,n} \sim \mathcal{CN}(\sqrt{\beta}h_{CB,n}s_n, N_o)$, if $x_n = 0$ and $r_{B,n}|x_n, x_{n-\Theta}, y_n, h_{CB,n} \sim \mathcal{CN}(\sqrt{\beta}h_{CB,n}s_n, N_{o\beta})$, if $x_n = 1$. Thus, using the distribution of $r_{B,n}$, the joint MAP decoder for Phase-III is

$$rCl\hat{i}, \hat{j}, \hat{m} = \arg \max_{i,j,m} g_{III} \left(r_{B,n}|x_n = i, x_{n-\Theta} = j, y_n = e^{j\frac{\pi}{M}(2m+1)}, h_{CB,n} \right), \quad (18)$$

where $i \in \{0, 1\}$, $j \in \{0, 1\}$, and $m \in \{0, \dots, M-1\}$. Further, $g_{III}(\cdot)$ is the conditional PDF of $r_{B,n}$, conditioned on $x_{n-\Theta}$, x_n , y_n , and $h_{CB,n}$. Along the similar lines of Phase-II, we note that $g_{III}(\cdot)$ in (18) is also a Gaussian mixture for various realizations of $x_{n-\Theta}$. Therefore, we approximate $g_{III}(\cdot)$ as $\tilde{g}_{III}(\cdot)$, where we retain the dominant terms from the Gaussian mixture, for $x_{n-\Theta} = 0$ and $x_{n-\Theta} = 1$, respectively. The JDD for Phase-III of 3ϕ DASC-MF is

$$rCl\hat{i}, \hat{j}, \hat{m} = \arg \max_{i,j,m} \tilde{g}_{III} \left(r_{B,n}|x_n = i, x_{n-\Theta} = j, y_n = e^{j\frac{\pi}{M}(2m+1)}, h_{CB,n} \right), \quad (19)$$

where $i, j \in \{0, 1\}$ and $m \in \{0, \dots, M-1\}$. In the next theorem, we compute a union bound on the probability of error in jointly decoding x_n , $x_{n-\Theta}$, and y_n , when using the JDD presented in (19).

TABLE II: ERROR TERMS FOR PHASE-III OF 3ϕ DASC-MF SCHEME AS GIVEN IN THEOREM 4

$P_{1,III} = e^{-\frac{\rho}{N_o}}$	$P_{2,III} = Q\left(\frac{ h_{CB,n} d_{III}}{\sqrt{2N_o}}\right)$	$P_{3,III} = Q_1\left(\frac{ A }{\sqrt{N_o/2}}, \frac{\sqrt{\xi_1}}{\sqrt{N_o/2}}\right)$
$P_{4,III} = 1 - e^{-\frac{\rho}{N_{o\beta}}}$	$P_{5,III} = Q\left(\frac{ h_{CB,n} d_{III}}{\sqrt{2N_{o\beta}}}\right)$	$P_{6,III} = 1 - Q_1\left(\frac{ B }{\sqrt{N_{o\beta}/2}}, \frac{\sqrt{\xi_2}}{\sqrt{N_{o\beta}/2}}\right)$
$P_{9,III} = Q_1\left(\frac{ A }{\sqrt{N_o/2}}, \frac{\sqrt{\xi_2}}{\sqrt{N_o/2}}\right)$	$P_{12,III} = 1 - Q_1\left(\frac{ B }{\sqrt{N_{o\beta}/2}}, \frac{\sqrt{\xi_1}}{\sqrt{N_{o\beta}/2}}\right)$	$P_{3,III} = Q_1\left(\frac{ B }{\sqrt{N_o/2}}, \frac{\sqrt{\xi_1}}{\sqrt{N_o/2}}\right)$
$P_{6,III} = 1 - Q_1\left(\frac{ A }{\sqrt{N_{o\beta}/2}}, \frac{\sqrt{\xi_2}}{\sqrt{N_{o\beta}/2}}\right)$	$P_{9,III} = Q_1\left(\frac{ B }{\sqrt{N_o/2}}, \frac{\sqrt{\xi_2}}{\sqrt{N_o/2}}\right)$	$P_{12,III} = 1 - Q_1\left(\frac{ A }{\sqrt{N_{o\beta}/2}}, \frac{\sqrt{\xi_1}}{\sqrt{N_{o\beta}/2}}\right)$

Theorem 4. At high SNR, the error probability for Phase-III, denoted by $P_{e,III}$, is upper bounded by

$$\frac{1}{4} \left[\Phi_{00}(P_{1,III}+2P_{2,III}+2P_{3,III}+P_{4,III}+2P_{5,III}+2P_{6,III}) + \Phi_{01}(P_{1,III}+2P_{2,III}+2P_{3,III}+P_{4,III}+2P_{5,III}+2P_{6,III}) + \Phi_{11}(P_{7,III}+2P_{8,III}+2P_{9,III}+P_{10,III}+2P_{11,III}+2P_{12,III}) + \Phi_{10}(P_{7,III}+2P_{8,III}+2P_{9,III}+P_{10,III}+2P_{11,III}+2P_{12,III}) \right], \quad (20)$$

where the various error terms in (20) are tabulated in Table II, such that, $P_{4,III} = P_{10,III} = P_{4,III} = P_{10,III}$; $P_{5,III} = P_{11,III} = 1 - P_{5,III} = 1 - P_{11,III}$; $P_{1,III} = P_{7,III} = P_{1,III} = P_{7,III}$; $P_{2,III} = P_{8,III} = 1 - P_{2,III} = 1 - P_{8,III}$.

Proof. This can be proved along the similar lines of Theorem 3. \square

In addition to the terms defined in Table II, $\varrho = \frac{N_o N_{o\beta}}{N_o - N_{o\beta}} \ln \left(\frac{N_o}{N_{o\beta}} \right)$ is the threshold for non-coherent energy detection at Bob between $(0, j, m)$ and $(1, j, m)$, $A = \frac{|h_{CB,n}| d_{III} N_o}{N_o - N_{o\beta}}$, $B = \frac{|h_{CB,n}| d_{III} N_{o\beta}}{N_o - N_{o\beta}}$, $\xi_1 = \frac{N_o N_{o\beta}}{N_o - N_{o\beta}} \left[\ln \left(\frac{N_o \Phi_{11}}{N_{o\beta} \Phi_{00}} \right) + \frac{|h_{CB,n}|^2 d_{III}^2}{N_o - N_{o\beta}} \right]$, and $\xi_2 = \frac{N_o N_{o\beta}}{N_o - N_{o\beta}} \left[\ln \left(\frac{N_o \Phi_{00}}{N_{o\beta} \Phi_{11}} \right) + \frac{|h_{CB,n}|^2 d_{III}^2}{N_o - N_{o\beta}} \right]$ are the parameters of the respective Marcum-Q functions ($Q_1(\cdot, \cdot)$), where $d_{III} = 2\sqrt{\beta} \sin \frac{\pi}{2M}$ is the minimum Euclidean distance between the constellation symbols received during Phase-III.

For $M = 4$, the various error terms in (20) are depicted in Fig. 5 (c). We note that the upper bound on $P_{e,III}$ in (20) contains exponential functions, Q-functions, and Marcum-Q functions. Although it is straightforward to compute the average of Q-functions over various realizations of $h_{CB,n}$ in closed-form, averaging Marcum-Q functions over various realizations of $h_{CB,n}$ is non-tractable for certain cases. Therefore, in the next lemma, we directly provide an upper bound on the Marcum-Q function averaged over the realizations of $h_{CB,n}$ to simplify the analysis.

Lemma 1. *The term $\mathbb{E}_{h_{CB,n}} [P_{3,III}]$ is upper bounded by $P_{1,III}$, for all $0 < \beta < 1$.*

Proof. Along the similar lines of [16], we compute $\mathbb{E}_{h_{CB,n}} [P_{3,III}] = \left(\frac{N_o \Phi_{11}}{N_{o\beta} \Phi_{00}} \right)^{\frac{N_{o\beta}}{N_{o\beta} - N_o}} \frac{(N_{o\beta} - N_o)^2}{(N_{o\beta} - N_o)^2 + d_{III}^2 N_{o\beta}}$. From the expression of Φ_{00} and Φ_{11} , we have $\Phi_{00} \geq \Phi_{11}$, thus, $\frac{\mathbb{E}_{h_{CB,n}} [P_{3,III}]}{P_{1,III}} \leq 1$. \square

In addition to Lemma 1, for moderate and high SNRs, we observe that, $\mathbb{E}_{h_{CB,n}} [P_{3,III}] \ll P_{1,III}$. Therefore, we use the upper bound $\mathbb{E}_{h_{CB,n}} [2P_{3,III}] \leq P_{1,III}$. Along the similar lines of Lemma 1, the following inequalities also hold good: $\mathbb{E}_{h_{CB,n}} [2P_{6,III}] \leq P_{4,III}$, $\mathbb{E}_{h_{CB,n}} [2P_{9,III}] \leq P_{7,III}$, and $\mathbb{E}_{h_{CB,n}} [2P_{12,III}] \leq P_{10,III}$. Furthermore, we also upper bound all the error terms that are the coefficients of Φ_{01} and Φ_{10} in (20) by 1, thereby circumventing the non-tractable issue of Marcum-Q functions.

Corollary 2. *If $P_{III,avg} = \mathbb{E}_{h_{CB,n}} [P_{e,III}]$ denotes the average probability of error over all the realizations of $h_{CB,n}$, then an upper bound on $P_{III,avg}$ is given as $\mathcal{P}_{III} \triangleq \frac{1}{2} \left(\Phi_{00} (P_{1,III} + P_{2,III}^* + P_{4,III} + P_{5,III}^*) + 5(\Phi_{01} + \Phi_{10}) + \Phi_{11} (P_{7,III} + P_{8,III}^* + P_{10,III} + P_{11,III}^*) \right)$, where $P_{2,III}^* = P_{8,III}^* = \frac{2N_o}{4N_o + d_{III}^2}$, $P_{5,III}^* = P_{11,III}^* = \frac{2N_{o\beta}}{4N_{o\beta} + d_{III}^2}$.*

D. Optimization of N_C and β for 3 ϕ DASC-MF Relaying Scheme

Substituting \mathcal{P}_I , \mathcal{P}_{III} , and \mathcal{P}_{III} from Theorem 2, Corollary 1, and Corollary 2, respectively in (6), we obtain an upper bound on the average probability of error of 3 ϕ DASC-MF, denoted by $\mathcal{P}_{e,3\phi}$ as

$$rClP_{e,3\phi} \leq \mathcal{P}_{e,3\phi} \triangleq \frac{\Theta}{L} \mathcal{P}_I + \frac{(L - 2\Theta)}{L} \mathcal{P}_{II} + \frac{\Theta}{L} \mathcal{P}_{III}. \quad (21)$$

Therefore, instead of solving (7), we solve an alternate optimization problem of minimising $\mathcal{P}_{e,3\phi}$ over the variables on interest, N_C and β . Thus, the modified optimization problem is given as

$$rClN_C^\dagger, \beta^\dagger = \arg \min_{N_C, \beta} \mathcal{P}_{e,3\phi}; \quad \text{s.t.: } N_C > 1, 0 < \beta < 1. \quad (22)$$

Unlike Phase-I and Phase-II, decoding in Phase-III is a combination of coherent and non-coherent detection. As a result, for a given N_C , β , and SNR, the error-rates for Phase-III dominates Phase-I and Phase-II, and thus, dominates $\mathcal{P}_{e,3\phi}$. Although, we can achieve improved error-rates during Phase-III by increasing N_C , we cannot indefinitely increase N_C , because Θ is an increasing function of N_C and for large values of N_C , the fraction of symbols decoded during Phase-III increases, which in turn increases $\mathcal{P}_{e,3\phi}$. Therefore, we must use an appropriate N_C that solves (22). Towards solving (22), we observe that proving unimodality of $\mathcal{P}_{e,3\phi}$ as a function of N_C and β is challenging due to the presence of the upper and the lower Gamma functions in the expressions of \mathcal{P}_{II} and \mathcal{P}_{III} . Therefore, in this section, we first fix N_C to analyse $\mathcal{P}_{e,3\phi}$ as a function of β and then propose a low-complexity algorithm to obtain the near-optimal values of N_C and β that minimizes $\mathcal{P}_{e,3\phi}$.

Towards minimising $\mathcal{P}_{e,3\phi}$, we observe that when we fix N_C and vary β , $\mathcal{P}_{e,3\phi}$ has a unique dip, for $\beta \in (0, 1)$. This is due to the fact that, when we fix $\alpha = 1 - \Delta N_o$ and N_C , \mathcal{P}_I and \mathcal{P}_{II} are independent of β , but \mathcal{P}_{III} has a unique dip for $\beta \in (0, 1)$. Further, we also observe that, the unique dip of \mathcal{P}_{III} is close to the intersection of the increasing and decreasing terms of \mathcal{P}_{III} . The above observation is exemplified in Fig. 6 for $\Theta = \lceil 10 \log_{10}(N_C) \rceil$ at SNR = 25 dB and $\Delta = 0.1$. Therefore, in the next lemma, we fix N_C and identify the increasing and decreasing terms in \mathcal{P}_{III} as a function of β . Subsequently, in Theorem 5, we show that the increasing and decreasing terms in \mathcal{P}_{III} intersect only once for $\beta \in (0, 1)$.

Lemma 2. *For a fixed α and N_C , if P_+ and P_- denote the increasing and decreasing terms in \mathcal{P}_{III} , respectively, w.r.t. β , then, $P_+ = \Phi_{00}(P_{1,III} + P_{4,III}) + \Phi_{11}(P_{7,III} + P_{10,III})$ and $P_- = \Phi_{00}(P_{2,III}^* + P_{5,III}^*) + \Phi_{11}(P_{8,III}^* + P_{11,III}^*)$.*

Proof. Along the similar lines of Remark 1, we can prove that the terms $P_{1,III}$, $P_{4,III}$, $P_{7,III}$, and $P_{10,III}$ are increasing functions of β . Further, since Φ_{00} and Φ_{11} are independent of β , $P_+ = \Phi_{00}(P_{1,III} + P_{4,III}) + \Phi_{11}(P_{7,III} + P_{10,III})$ is an increasing function of β .

Further, the expressions of $P_{2,III}^*$, $P_{5,III}^*$, $P_{8,III}^*$, and $P_{11,III}^*$ are such that, $P_{2,III}^* = P_{8,III}^* = \frac{2N_o}{4N_o + d_{III}^2}$ and $P_{5,III}^* = P_{11,III}^* = \frac{2N_o\beta}{4N_o\beta + d_{III}^2}$. Differentiating $P_{2,III}^*$ w.r.t. β we get, $-\frac{2N_o}{(4N_o + d_{III}^2)^2} \sin^2 \frac{\pi}{2M}$. Therefore, $P_{2,III}^*$ and $P_{8,III}^*$ are decreasing functions of β . Along similar lines, we can prove that $P_{5,III}^*$ and $P_{11,III}^*$ are decreasing functions of β . Thus, we have $P_- = \Phi_{00}(P_{2,III}^* + P_{5,III}^*) + \Phi_{11}(P_{8,III}^* + P_{11,III}^*)$. \square

Theorem 5. *For a fixed α and N_C , P_+ and P_- intersect only once for $\beta \in (0, 1)$.*

Proof. This can be proved along the similar lines of [16, Theorem 3]. \square

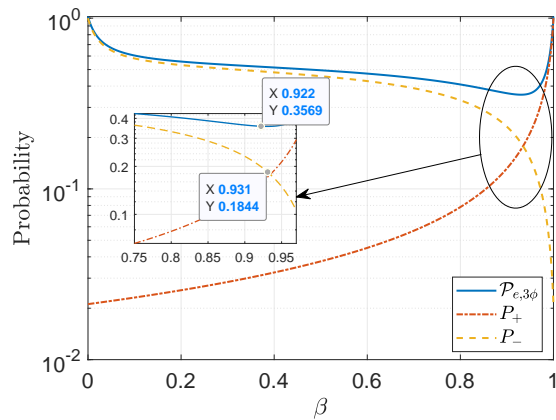


Fig. 6: Variation of $\mathcal{P}_{e,3\phi}$ and its increasing and decreasing terms as a function of β at 25 dB.

Algorithm 1. N_C - β Optimization

Input: $\mathcal{P}_{e,3\phi}$, P_+ , P_- , Δ , SNR , δ_{tol}

Output: N_C^\dagger , β^\dagger

```

1  $\beta \leftarrow \beta_o$ ;
2  $N_C \leftarrow 1$ ;
3  $P_o = 0.5$ ;
4 while true do
5   Use NR algorithm to compute
   intersection of  $P_+$  and  $P_-$ , denoted by
    $\beta_{int}$ ;
6   Substitute  $\beta_{int}$  in  $\mathcal{P}_{e,3\phi}$  and compute
    $P_{eval}$ ;
7   if  $|P_o - P_{eval}| > \delta_{tol}$  then
8      $N_C \leftarrow N_C + 1$ ;
9      $\beta_o \leftarrow \beta_{int}$ ;
10     $P_o \leftarrow P_{eval}$ 
11  else
12     $N_C^\dagger = N_C$ ;
13     $\beta^\dagger = \beta_{int}$ 
14  end
15 end

```

Remark 3. *The unique intersection of P_+ and P_- can be computed using the Newton-Raphson (NR) algorithm.*

Using the insights of Lemma 2 and Theorem 5, we now present a low-complexity algorithm in Algorithm 1, referred to as the N_C - β Optimization algorithm, which provides a local minima of $\mathcal{P}_{e,3\phi}$ over the variables, N_C and β . We start the algorithm with $N_C = 1$, an initial estimate of $\mathcal{P}_{e,3\phi}$, denoted by P_o , and an initial estimate of the intersection of P_+ and P_- , denoted by β_o . We use the NR algorithm to compute the intersection of P_+ and P_- as β_{int} and evaluate P_{eval} by substituting N_C and β_{int} in $\mathcal{P}_{e,3\phi}$. We iteratively compute β_{int} by incrementing N_C in steps of 1 until the absolute value of the difference between P_{eval} and P_o is less than the tolerance value, δ_{tol} . When $|P_o - P_{eval}| < \delta_{tol}$, we exit the while-loop with the near-optimal values of N_C and β , denoted by N_C^\dagger and β^\dagger , respectively.

V. SEMI-COHERENT MULTIPLE ACCESS CHANNEL SCHEME

A major limitation of the 3ϕ DASC-MF scheme proposed in the previous section is that when $\Theta > \frac{L}{2}$, only a fraction of Alice's symbols can be recovered using the multiplexed symbols within the deadline and a majority of the multiplexed symbols are received at Bob after the deadline, resulting in violation of the latency constraint. As a result, when $\Theta > \frac{L}{2}$, Alice and Charlie must resort to uncoordinated multiple access communication, wherein Alice and Charlie transmit their symbols using $1 - \varepsilon$ and ε fractions of their energies, respectively, on f_{CB} over the MAC, where $\varepsilon \in (0, 1)$ is the design parameter under consideration. Here, Charlie does not decode Alice's symbol and only transmits his M -PSK symbols. Subsequently, Bob uses the received symbols to jointly decode Alice's and Charlie's symbols. A major distinction between the 3ϕ DASC-MF scheme and SC-MAC is that due to no knowledge of Alice's symbols, Charlie always scales his constellation by energy ε . This

phenomenon is similar to Phase-III 3ϕ DASC-MF scheme. Furthermore, since the Alice-to-Bob link of the MAC is non-coherent and Charlie-to-Bob link of the MAC is coherent, we refer to this scheme as the Semi-Coherent Multiple Access Channel (SC-MAC). Subsequently, similar to the 3ϕ DASC-MF scheme, Alice and Charlie transmit dummy OOK symbols from a Gold-sequence based scrambler with ε and $1 - \varepsilon$ fractions of their energies, respectively, on f_{AB} to evade the ED.

A. Error Analysis of SC-MAC

If $x_n \in \{0, 1\}$ and $y_n \in \mathcal{S}_C$ denote the OOK and M -PSK symbols of Alice and Charlie, respectively, then the received symbol at Bob, assuming symbol level synchronization, is given by

$$rClr_{B,n} = \sqrt{1 - \varepsilon}h_{AB,n}x_n + \sqrt{\varepsilon}h_{CB,n}y_n + w_{B,n}, \quad 1 \leq n \leq L, \quad (23)$$

where $h_{AB,n}$, $h_{CB,n}$, and $w_{B,n}$ are as defined in previous sections. Unlike 3ϕ DASC-MF, $r_{B,n}$ in SC-MAC are independent across time, therefore, we drop the subscript n from the variables during the error analysis of SC-MAC. Owing to the non-coherent nature of Alice-to-Bob link of the MAC and coherent nature of the Charlie-to-Bob link of the MAC, and the Gaussian statistics of the channels and the noise, the distribution of r_B conditioned on x and y as $r_B|x,y,h_{CB} \sim \mathcal{CN}(\sqrt{\varepsilon}h_{CB}y, N_o)$, if $x = 0$ and $r_B|x,y,h_{CB} \sim \mathcal{CN}(\sqrt{\varepsilon}h_{CB}y, N_{o\varepsilon})$, if $x = 1$. Using the distribution of r_B , the joint MAP decoder for SC-MAC is

$$rCl\hat{i}, \hat{m} = \arg \max_{i,m} g_{MAC} \left(r_B|x = i, y = e^{j\frac{\pi}{M}(2m+1)}, h_{CB} \right), \quad (24)$$

where $i \in \{0, 1\}$ and $m \in \{0, \dots, M - 1\}$ and g_{MAC} is the PDF of r_B conditioned on x , y , and h_{CB} . If Alice and Charlie transmit OOK and M -PSK, then a transmitted pair is denoted by (i, m) . Fig. 7 depicts the constellation diagram at Bob jointly contributed by Alice and Charlie when using SC-MAC scheme with $M = 4$. When $x_n = 1$ and $x_n = 0$, the effective variance of the noise at Bob is $N_o + 1 - \varepsilon$ and N_o , respectively. The *square box* denotes the symbols with variance N_o and *circular disks* represent the symbols with variance $N_{o\varepsilon} = N_o + 1 - \varepsilon$. In the next section, we discuss the error analysis of the SC-MAC scheme.

TABLE III: ERROR TERMS FOR SC-MAC AS GIVEN IN THEOREM 6

$P_{1,MAC} = 1 - e^{-\frac{\psi}{N_o}}$	$P_{2,MAC} = Q_1 \left(\frac{ C }{\sqrt{N_o/2}}, \frac{\sqrt{\eta}}{\sqrt{N_o/2}} \right)$	$P_{3,MAC} = Q \left(\frac{ h_{CB,n} d}{\sqrt{2N_o}} \right)$
$P_{4,MAC} = e^{-\frac{\psi}{N_{o\varepsilon}}}$	$P_{5,MAC} = 1 - Q_1 \left(\frac{ D }{\sqrt{N_{o\varepsilon}/2}}, \frac{\sqrt{\eta}}{\sqrt{N_{o\varepsilon}/2}} \right)$	$P_{6,MAC} = Q \left(\frac{ h_{CB,n} d}{\sqrt{2N_{o\varepsilon}}} \right)$

Theorem 6. *At high SNR, a union bound on probability of error for SC-MAC is approximated as*

$$rCl\frac{1}{2} (P_{1,MAC} + 2P_{2,MAC} + 2P_{3,MAC} + P_{4,MAC} + 2P_{5,MAC} + 2P_{6,MAC}), \quad (25)$$

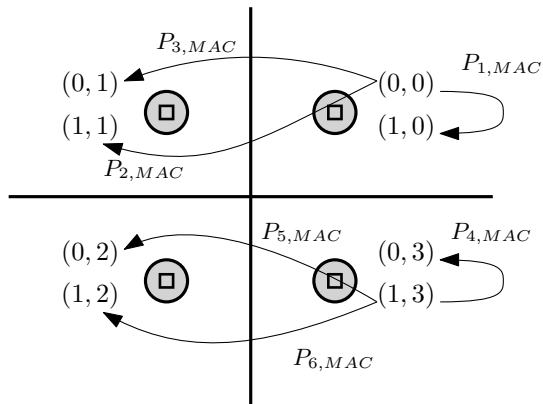


Fig. 7: Constellation diagram jointly contributed by Alice and Charlie when using SC-MAC.

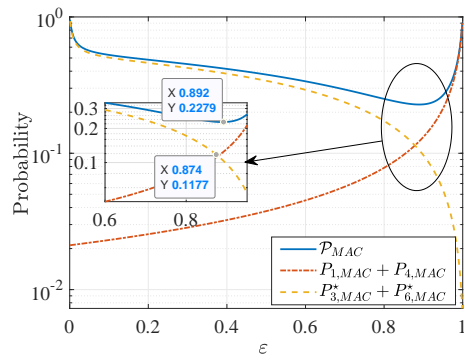


Fig. 8: Variation of \mathcal{P}_{MAC} and its increasing and decreasing terms as a function of ε at 25 dB.

where the various error terms in (25) are tabulated in Table III. Further, $\psi = \frac{N_o N_{o\varepsilon}}{N_o - N_{o\varepsilon}} \ln \left(\frac{N_o}{N_{o\varepsilon}} \right)$, $C = \frac{|h_{CB,n}| d N_o}{N_o - N_{o\varepsilon}}$, $D = \frac{|h_{CB,n}| d N_{o\varepsilon}}{N_o - N_{o\varepsilon}}$, and $\eta = \frac{N_o N_{o\varepsilon}}{N_o - N_{o\varepsilon}} \left[\ln \left(\frac{N_o}{N_{o\varepsilon}} \right) + \frac{|h_{CB,n}|^2 d^2}{N_o - N_{o\varepsilon}} \right]$ are the parameters of the Marcum- Q function, where, $d = 2\sqrt{\varepsilon} \sin \frac{\pi}{M}$ denotes the minimum Euclidean distance between the constellation points received at Bob.

Proof. Let a pair corresponding to the symbols x and y be denoted by (i, m) . Let $\nabla_{(i,m) \rightarrow (i',m')}$ be the event $(i, m) \neq (i', m')$, then a transmitted pair (i, m) is incorrectly decoded as (i', m') if

$$rCl \nabla_{(i,m) \rightarrow (i',m')} \triangleq \frac{g_{MAC} \left(r_B | x = i, y = e^{j\frac{\pi}{M}(2m+1)}, h_{CB} \right)}{g_{MAC} \left(r_B | x = i', y = e^{j\frac{\pi}{M}(2m'+1)}, h_{CB} \right)} \leq 1. \quad (26)$$

Therefore, the probability of decoding a transmitted pair (i, m) as (i', m') is given as $\Pr((i, m) \rightarrow (i', m')) = \Pr \left(\nabla_{(i,m) \rightarrow (i',m')} \leq 1 \right)$. If $\Pr \left((\hat{i}, \hat{m}) \neq (i, m) \right)$ denotes the overall probability of error in decoding a transmit pair (i, m) , then $\Pr \left((\hat{i}, \hat{m}) \neq (i, m) \right)$ is upper bounded as

$$rCl \Pr \left((\hat{i}, \hat{m}) \neq (i, m) \right) \leq \sum_{\substack{i'=0 \\ (i,m) \neq (i',m')}}^1 \sum_{m'=0}^{M-1} \Pr \left(\nabla_{(i,m) \rightarrow (i',m')} \right), \quad (27)$$

where (\hat{i}, \hat{m}) is the decoded pair at Bob, corresponding to the transmitted pair (i, m) . Thus, if $P_{e,MAC}$ denotes the overall probability of error for $2M$ symbols, then $P_{e,MAC}$ is upper bounded as $P_{e,MAC} \leq \frac{1}{2M} \sum_{i=0}^1 \sum_{m=0}^{M-1} M \Pr((\hat{i}, \hat{m}) \neq (i, m))$. Finally, considering the nearest-neighbours at high SNR, $P_{e,MAC}$ is approximated as (25), where the various error terms in (25) are tabulated in Table III. Furthermore, these terms are also depicted in Fig. 7 for 4-PSK used by Charlie. \square

Corollary 3. Using the results of Lemma 1, we upper bound $P_{2,MAC}$ and $P_{3,MAC}$ as $2P_{2,MAC} \leq P_{1,MAC}$ and $2P_{3,MAC} \leq P_{4,MAC}$. Further, using the Chernoff bound on the Q -functions and averaging $P_{e,MAC}$ over the realisations of h_{CB} , we get $\mathbb{E}_{h_{CB}}[P_{e,MAC}] \leq \mathcal{P}_{MAC} \triangleq P_{1,MAC} + P_{3,MAC}^* + P_{4,MAC} + P_{6,MAC}^*$, where $P_{3,MAC}^* = \frac{2N_o}{4N_o + d^2}$ and $P_{6,MAC}^* = \frac{2N_{o\varepsilon}}{4N_{o\varepsilon} + d^2}$.

While observing (23), we notice that when $\varepsilon \rightarrow 1$, Alice's symbols are transmitted with lower

energy, whereas Charlie transmits his symbols with higher energy. However, when $\varepsilon \rightarrow 0$, Alice's symbols are transmitted with higher energy as compared to Charlie. Thus, in the extreme range, the joint error-rates at Bob are expected to be high and therefore, Alice and Charlie must use a value of ε that minimizes the error-rates at Bob. Towards minimizing \mathcal{P}_{MAC} at Bob, we pose an optimization problem as given below.

$$rCl\varepsilon^\dagger = \arg \min_{\varepsilon} \mathcal{P}_{MAC}; \quad \text{s.t.: } 0 < \varepsilon < 1. \quad (28)$$

Towards minimizing \mathcal{P}_{MAC} , we note that, it is straightforward to prove that \mathcal{P}_{MAC} is a sum of increasing and decreasing terms w.r.t. ε . In particular, using the results of Lemma 2, we notice that $P_{1,MAC} + P_{4,MAC}$ is an increasing function of ε and $P_{3,MAC}^* + P_{6,MAC}^*$ is a decreasing function of ε and the intersection of the increasing and decreasing terms is close to the unique minima of \mathcal{P}_{MAC} . This observation is exemplified in Fig. 8 at SNR = 25 dB. Along the similar lines of Theorem 5, it is straightforward to prove that, $P_{1,MAC} + P_{4,MAC}$ and $P_{3,MAC}^* + P_{6,MAC}^*$ intersect at a unique value of $\varepsilon \in (0, 1)$. Therefore, the unique intersection of $P_{1,MAC} + P_{4,MAC}$ and $P_{3,MAC}^* + P_{6,MAC}^*$ can be computed using the NR algorithm. In the next section, we present Monte-Carlo simulations for SC-MAC scheme and showcase its error performance.

VI. SIMULATION RESULTS ON THE 3ϕ DASC-MF AND SC-MAC SCHEMES

In this section, we present simulation results for the two schemes proposed in the previous sections. The simulation parameters for the Monte-Carlo simulations are as follows: We assume 4-PSK signalling at Charlie and OOK signalling at Alice. All the links in the network are Rayleigh faded, such that $\sigma_{AB}^2 = \sigma_{CB}^2 = 1$ and $\sigma_{AC}^2 = 4$, thus providing 6 dB improvement in SNR on Alice-to-Charlie link as compared to Alice-to-Bob link of the MAC. Further, we assume Bob has the perfect channel estimates of Charlie-to-Bob link on f_{CB} . Furthermore, all the channels and noise realizations are statistically independent. Finally, the variance of the AWGN at Bob and Charlie is $N_o = SNR^{-1}$. For the 3ϕ scheme, we use $L = 200$ and $\Delta = 0.1$ along with the following three delay models, i.e., $\Theta = \lceil 10 \log N_C^\dagger \rceil$, $\Theta = \lceil \log_2 N_C^\dagger \rceil$, and $\Theta = \lceil \frac{L}{2} \rceil$. Since, Θ is a function of the FD architecture of Charlie, similar results can be generated for any model on Θ , as long as, $\Theta \leq \frac{L}{2}$.

TABLE IV: VALUES OF $(N_C^\dagger, \beta^\dagger)$ USING EXACT AND INTERSECTION METHODS FOR VARIOUS Θ

$\downarrow \Theta \setminus \begin{matrix} \text{SNR} \\ \rightarrow \end{matrix}$	21 dB		25 dB		29 dB	
	$(N_C^\dagger, \beta^\dagger)_{EM}$	$(N_C^\dagger, \beta^\dagger)_{Int}$	$(N_C^\dagger, \beta^\dagger)_{EM}$	$(N_C^\dagger, \beta^\dagger)_{Int}$	$(N_C^\dagger, \beta^\dagger)_{EM}$	$(N_C^\dagger, \beta^\dagger)_{Int}$
$\lceil 10 \log_{10} N_C \rceil$	(125,0.8730)	(125, 0.9020)	(127,0.9220)	(127,0.9310)	(129, 0.9580)	(129, 0.9570)
$\lceil \log_2 N_C \rceil$	(126,0.8730)	(126, 0.9020)	(128,0.9220)	(128,0.9310)	(130, 0.9580)	(130, 0.9570)
$\lceil \sqrt{N_C} \rceil$	(122,0.8730)	(122, 0.9020)	(127,0.9220)	(127,0.9310)	(129, 0.9580)	(129, 0.9570)

TABLE V: VALUES OF (N_C^*, β^*) OBTAINED USING EXHAUSTIVE METHOD FOR VARIOUS Θ

$\downarrow \Theta \setminus \overrightarrow{SNR}$	21 dB	25 dB	29 dB
$\lceil 10 \log_{10} N_C \rceil$	(125, 0.8700)	(127, 0.9290)	(129, 0.9430)
$\lceil \log_2 N_C \rceil$	(126, 0.8700)	(128, 0.9290)	(130, 0.9430)
$\lceil \sqrt{N_C} \rceil$	(122, 0.8700)	(127, 0.9290)	(129, 0.9430)

TABLE VI: VALUES OF ε OBTAINED USING EXHAUSTIVE AND INTERSECTION METHODS FOR SC-MAC

$\downarrow \varepsilon \setminus \overrightarrow{SNR}$	19 dB	21 dB	25 dB	29 dB
$\varepsilon_{\text{ES}}^*$	0.8080	0.8700	0.8920	0.9250
$\varepsilon_{\text{Int}}^\dagger$	0.7820	0.8510	0.8740	0.9190

To present the error performance of the 3ϕ scheme, we first compute the near-optimal values of (N_C, β) using the following three methods: i) an Exhaustive Search (ES), ii) an Exact Method (EM), and iii) the N_C - β Optimization algorithm. For the ES, we use Monte-Carlo simulations to empirically compute the overall probability of error in (6) and then exhaustively search for (N_C^*, β^*) that minimises (6), for a given Θ and SNR. The step size for N_C is one and that for $\beta \in (0, 1)$ is 10^{-3} . For the EM, we use the upper bounds proposed in Corollary 1 and Corollary 2 and exhaustively search for $(N_C^\dagger, \beta^\dagger)$ that minimises (21), for a given Θ and SNR. Here, the resolution of β is same as used for the ES. Finally, we compute $(N_C^\dagger, \beta^\dagger)$ using the N_C - β Optimization algorithm, as explained in Algorithm 1. In Table IV, we tabulate N_C^\dagger and β^\dagger for various combinations of Θ and SNR using the EM and N_C - β Optimization algorithm. Further, for the same Θ and SNR, in Table V, we also tabulate N_C^\dagger and β^\dagger obtained using the ES. From Table IV and Table V we observe that the obtained values of N_C and β are close. Further, we also observe that the required value of N_C^\dagger increases with SNR. This is due to the fact that, although we have upper bounded the interference from Alice on Alice-to-Bob link of the MAC by ΔN_o , Charlie uses the same energy, ΔN_o to decode Alice's symbols. Therefore, as SNR increases, N_o decreases, and Charlie requires more receive-antennas to faithfully decode Alice's symbols. Along the similar lines, for the SC-MAC scheme, we tabulate ε obtained using the ES method and the intersection method, for various SNRs in Table VI. For ES we exhaustively search for the value of $\varepsilon \in (0, 1)$ (in the steps of 10^{-3}) that minimises the empirically computed average probability of error. From the table we infer that ε obtained using both the methods are close.

In Fig. 9, we plot the Joint Symbol Error Rate (SER), i.e., the joint error performance of Alice and Charlie, at Bob when using the 3ϕ DASC-MF scheme (for various models on Θ) and SC-MAC scheme, as a function of SNR. In 3ϕ DASC-MF, for each model, we first obtain the value of (N_C, β) pair using the ES, EM, and N_C - β Optimization Algorithm and then obtain the value of Joint SER through Monte-Carlo simulations. Along the similar lines, for SC-MAC scheme, we first obtain the value of ε using the ES method and the intersection method and then compute the Joint SER. It is evident that the Joint SER for both the schemes reduces as a function of SNR. We also note that among the three models considered for 3ϕ DASC-MF scheme, the error performance is best when $\Theta = \lceil \log_2 N_C^\dagger \rceil$ as

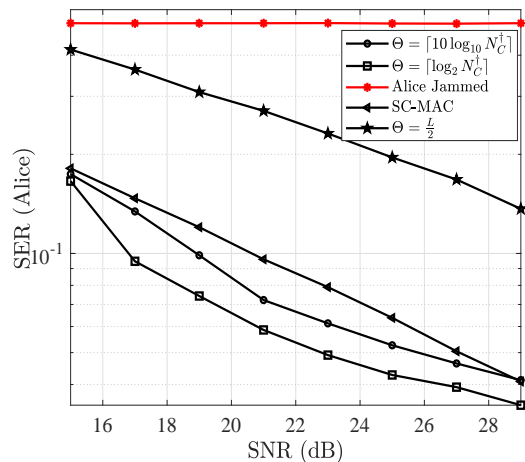
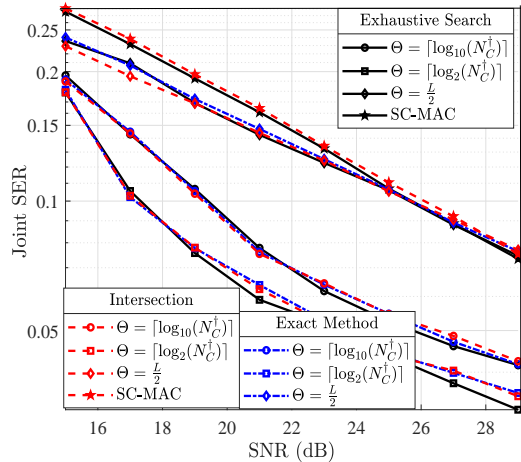


Fig. 9: Joint SER when using 3ϕ DASC-MF and SC-MAC. Fig. 10: SER (Alice) using 3ϕ DASC-MF and SC-MAC.

$\frac{\Theta}{L}$ is minimum when $\Theta = \lceil \log_2 N_C^\dagger \rceil$, thereby reducing the fraction of symbols decoded during Phase III. Additionally, when comparing SC-MAC and 3ϕ DASC-MF scheme, we note that SC-MAC is sub-optimal for the assumed models on Θ . This is because, throughout 3ϕ DASC-MF scheme, Bob decodes a majority of Alice's symbols using the coherent Charlie-to-Bob link of the MAC, whereas, in SC-MAC, Bob decodes all Alice's symbols using the non-coherent Alice-to-Bob link of the MAC. Thus, Alice's symbols in SC-MAC are decoded more reliably than 3ϕ DASC-MF.

Finally, in Fig. 10, we plot the improvement in Alice's error performance before and after implementing the proposed schemes. It is interesting to note that although the joint error performance of SC-MAC is inferior to 3ϕ DASC-MF when $\Theta = \frac{L}{2}$, SC-MAC outperforms 3ϕ DASC-MF when $\Theta = \frac{L}{2}$ when considering only Alice's SER at Bob. This is because, in SC-MAC, Bob decodes two symbols i.e., Alice's current symbols and Charlie's current symbol during the entire duration. In contrast, when $\Theta = \frac{L}{2}$, Bob decodes three symbols, i.e, Alice current symbol, Charlie's current symbol and Alice's symbol delayed by Θ symbols. As a result, the error rates for Alice are high for $\Theta = \frac{L}{2}$. Overall, it is clear from the plots that SC-MAC helps Alice to evade the jamming attack from Dave within the latency constraint, however, it is sub-optimal as compared to 3ϕ DASC-MF scheme. Nevertheless, it is a still a good option when $\Theta \geq \frac{L}{2}$.

VII. COVERTNESS ANALYSIS

As discussed in Sec. II, Dave uses an ED to detect the changes in the average energy level on all the frequencies in the network after the jamming attack. Since Alice and Charlie use f_{AB} and f_{CB} to execute the countermeasures, we restrict our analysis to these frequencies only. Thus, in the context of this work, we refer to a mitigation scheme as covert if Dave is unable to detect changes in the average energy levels of f_{AB} and f_{CB} . Further, throughout this section, we assume that Dave has the knowledge of the channel statistics of Alice-to-Dave link and Charlie-to-Dave link, but no knowledge of the channel coefficients of these links.

A. Covertness Analysis for ED when using 3 ϕ DASC-MF Relaying Scheme

In this section, we first discuss energy detection at Dave on f_{AB} and f_{CB} when using 3 ϕ DASC-MF and then, compute probability of false-alarms and probability of miss-detections on f_{AB} and f_{CB} . Before executing the jamming attack, Dave collects a frame of L symbols on f_{AB} and f_{CB} and computes their average energy. The n^{th} symbol received at Dave, before the jamming attack on f_{AB} and f_{CB} are respectively given as

$$rClr_{D,AB,n} = h_{AD,n}x_n + w_{D,AB,n}, \quad 1 \leq n \leq L, \quad (29)$$

$$r_{D,CB,n} = h_{CD,n}y_n + w_{D,CB,n}, \quad 1 \leq n \leq L, \quad (30)$$

where $h_{AD,n} \sim \mathcal{CN}(0, 1)$ and $h_{CD,n} \sim \mathcal{CN}(0, 1+\partial)$ are the n^{th} channel coefficients of Alice-to-Dave link and Charlie-to-Dave link, respectively, such that, ∂ captures the relative difference in the variance of Alice-to-Dave link and Charlie-to-Dave link. Further, $w_{D,AB,n} \sim \mathcal{CN}(0, \tilde{N}_o)$ is the effective AWGN at Dave on f_{AB} , such that, $\tilde{N}_o = N_o + \sigma_{DD}^2$, where σ_{DD}^2 is the variance of the residual SI at Dave and N_o is the variance of the AWGN at Dave. Furthermore, $w_{D,CB,n} \sim \mathcal{CN}(0, N_o)$ is the AWGN at Dave on f_{CB} . Since $r_{D,AB,n}$ and $r_{D,CB,n}$ are statistically independent over n , using weak law of large numbers, $\frac{1}{L} \sum_{n=1}^L |r_{D,AB,n}|^2 \rightarrow \mathcal{E}_{AB}$ and $\frac{1}{L} \sum_{n=1}^L |r_{D,CB,n}|^2 \rightarrow \mathcal{E}_{CB}$, in probability, such that $\mathcal{E}_{AB} = \tilde{N}_o + 0.5$ and $\mathcal{E}_{CB} = N_o + 1 + \partial$. However, due to short packet length, the measured average energies on f_{AB} and f_{CB} are not equal to \mathcal{E}_{AB} and \mathcal{E}_{CB} . Therefore, if \mathcal{H}_0 denotes the hypothesis that no countermeasure is implemented, then, probability of false-alarms on f_{AB} and f_{CB} are defined as follows.

Definition 1. The probability of false-alarm on f_{AB} , denoted by, $\mathbf{P}_{FA,AB}$ is given as $\mathbf{P}_{FA,AB} = \Pr(|\mathcal{U}_{L,AB} - \mathcal{E}_{AB}| \geq \nu_{AB} | \mathcal{H}_0 \text{ true})$, where, $\mathcal{U}_{L,AB}$ denotes the random variable (RV) corresponding to the average energy of L symbols received at Dave on f_{AB} and $\nu_{AB} > 0$ is a parameter of Dave's choice.

Definition 2. The probability of false-alarm on f_{CB} , denoted by, $\mathbf{P}_{FA,CB}$ is given as $\mathbf{P}_{FA,CB} = \Pr(|\mathcal{U}_{L,CB} - \mathcal{E}_{CB}| \geq \nu_{CB} | \mathcal{H}_0 \text{ true})$, for $\nu_{CB} > 0$, where, $\mathcal{U}_{L,CB}$ denotes the RV corresponding to the average energy of L symbols received at Dave on f_{CB} and ν_{CB} is a parameter of Dave's choice.

When $\tilde{N}_o \ll 1$, the distribution of $\mathcal{U}_{L,AB}$ is approximated as $\frac{1}{2^L} \sum_{l=0}^L \binom{L}{l} G(l, \frac{1}{L})$, where $G(\cdot, \cdot)$ denotes the Gamma distribution [19, Theorem 5]. Along the similar lines, when $N_o \ll 1$, the distribution of $\mathcal{U}_{L,CB}$ can be approximated as $\frac{1}{2^L} \sum_{l=0}^L \binom{L}{l} G(l, \frac{1+\partial}{L})$. Thus, the expressions of $\mathbf{P}_{FA,AB}$ and $\mathbf{P}_{FA,CB}$ when $\tilde{N}_o \ll 1$ and $N_o \ll 1$, respectively, are approximated as

$$rCl\mathbf{P}_{FA,AB} \approx \frac{1}{2^L} \left[\sum_{l=0}^L \binom{L}{l} \frac{\gamma(l, L(\mathcal{E}_{AB} - \nu_{AB}))}{\Gamma(l)} + \sum_{l=0}^L \binom{L}{l} \frac{\Gamma(l, L(\mathcal{E}_{AB} + \nu_{AB}))}{\Gamma(l)} \right], \quad (31)$$

$$\mathbf{P}_{FA,CB} \approx \frac{1}{2^L} \left[\sum_{l=0}^L \binom{L}{l} \frac{\gamma(l, \frac{L}{1+\partial}(\mathcal{E}_{CB} - \nu_{CB}))}{\Gamma(l)} + \sum_{l=0}^L \binom{L}{l} \frac{\Gamma(l, \frac{L}{1+\partial}(\mathcal{E}_{CB} + \nu_{CB}))}{\Gamma(l)} \right], \quad (32)$$

where ν_{AB} and ν_{CB} are decided by Dave. However, small values of ν_{AB} and ν_{CB} often result in high false-alarms, and large values of ν_{AB} and ν_{CB} result in high miss-detection. Thus, the values of ν_{AB} and ν_{CB} must be cautiously chosen by Dave so as to minimize both probability of false-alarm and probability of miss-detection. In the rest of the section, we discuss the probability of miss-detection on f_{AB} and f_{CB} , when using 3ϕ DASC-MF scheme for a given choice of ν_{AB} and ν_{CB} . Towards computing the probability of miss-detection, we first present the symbols observed at Dave on f_{AB} and then characterise the probability of miss-detection on f_{AB} . Along the similar lines, we will then characterise the probability of miss-detection on f_{CB} . We recall that Alice and Charlie use OOK symbols from a pre-shared Gold-sequence to cooperatively pour their residual energies on f_{AB} . Therefore, if $b_n \in \{0, 1\}$ denotes the n^{th} OOK bit jointly transmitted by Alice and Charlie, and $r_{D,AB,n}^\dagger$ denotes the n^{th} baseband symbol received at Dave, then

$$r_{D,AB,n}^\dagger = \begin{cases} \sqrt{\alpha}h_{AD,n}b_n + \sqrt{1-\alpha}h_{CD,n}b_n + w_{D,AB,n}, & \text{if } 1 \leq n \leq L - \Theta, \end{cases} \quad (33a)$$

$$r_{D,AB,n}^\dagger = \begin{cases} \sqrt{\beta^\dagger}h_{AD,n}b_n + \sqrt{1-\beta^\dagger}h_{CD,n}b_n + w_{D,AB,n}, & \text{if } L - \Theta + 1 \leq n \leq L. \end{cases} \quad (33b)$$

Let \mathcal{H}_1 denote the hypothesis that a countermeasure is implemented, then, formally, the probability of miss-detection at Dave on f_{AB} is given as follows.

Definition 3. Let $\mathcal{V}_{L,AB}$ denote the RV corresponding to the average energy of L symbols on f_{AB} after using 3ϕ DASC-MF scheme. Thus, probability of miss-detection denoted by, $\mathbf{P}_{MD,AB}^{3\phi}$, is $\mathbf{P}_{MD,AB}^{3\phi} = \Pr(|\mathcal{V}_{L,AB} - \mathcal{E}_{AB}| \leq \nu_{AB} | \mathcal{H}_1 \text{ true})$, for $\nu_{AB} > 0$.

Using (33a) and (33b), we will now characterize $\mathbf{P}_{MD,AB}^{3\phi}$. Let $v_{n_1,AB}$ denote the RV corresponding to $|r_{D,AB,n_1}^\dagger|^2$, such that $1 \leq n_1 \leq L - \Theta$ and $v_{n_2,AB}$ denote the RV corresponding to $|r_{D,AB,n_2}^\dagger|^2$, such that $L - \Theta + 1 \leq n_2 \leq L$. Thus, $\mathcal{V}_{L,AB} = \mathcal{V}_{L_1,AB} + \mathcal{V}_{L_2,AB}$, such that $\mathcal{V}_{L_1,AB} = \frac{1}{L} \sum_{n_1=1}^{L-\Theta} v_{n_1,AB}$ and $\mathcal{V}_{L_2,AB} = \frac{1}{L} \sum_{n_2=L-\Theta+1}^L v_{n_2,AB}$. In the next lemma, we compute the PDF of $\mathcal{V}_{L_1,AB}$ and $\mathcal{V}_{L_2,AB}$.

Lemma 3. When $\tilde{N}_o \ll 1$, the distribution of $\mathcal{V}_{L_1,AB}$ is approximated as $\frac{1}{2^{L-\Theta}} \sum_{l=0}^{L-\Theta} \binom{L-\Theta}{l} \mathbf{G}\left(l, \frac{\mathcal{A}}{L}\right)$, where $\mathcal{A} = \alpha + (1-\alpha)(1+\partial)$. Similarly, the distribution of $\mathcal{V}_{L_2,AB}$ is approximated as $\frac{1}{2^\Theta} \sum_{l=0}^{\Theta} \binom{\Theta}{l} \mathbf{G}\left(l, \frac{\mathcal{B}}{L}\right)$, where $\mathcal{B} = \beta^\dagger + (1-\beta^\dagger)(1+\partial)$.

Finally, $\frac{1}{2^{L-\Theta}} \sum_{l=0}^{L-\Theta} \binom{L-\Theta}{l} \mathbf{G}\left(l, \frac{\mathcal{A}}{L}\right) * \frac{1}{2^\Theta} \sum_{l=0}^{\Theta} \binom{\Theta}{l} \mathbf{G}\left(l, \frac{\mathcal{B}}{L}\right)$ gives the distribution of $\mathcal{V}_{L,AB}$, where $*$ denotes linear convolution. Using the distribution of $\mathcal{V}_{L,AB}$, it is straightforward to compute $\mathbf{P}_{MD,AB}^{3\phi}$.

Remark 4. If $\partial = 0$, then $\mathbf{P}_{FA,AB} + \mathbf{P}_{MD,AB}^{3\phi} = 1$ for all $\nu_{AB} > 0$.

Although, Remark 4 theoretically guarantees that $\mathbf{P}_{FA,AB} + \mathbf{P}_{MD,AB}^{3\phi} = 1$, in Sec. VII-C, through Monte-Carlo simulations, we show that, $\mathbf{P}_{FA,AB} + \mathbf{P}_{MD,AB}^{3\phi}$ is close to 1 for various values of ∂ .

We now compute the probability of miss-detection on f_{CB} , denoted by, $\mathbf{P}_{MD,CB}^{3\phi}$. Towards com-

putting $\mathbf{P}_{MD,CB}^{3\phi}$, we first observe the symbol received at Dave on f_{CB} , denoted by $r_{D,CB,n}^\dagger$ and then characterise its PDF. Thus, the n^{th} baseband symbol received at Dave on f_{CB} is given as

$$r_{D,CB,n}^\dagger = \begin{cases} \sqrt{1-\alpha}h_{AD,n}x_n + \sqrt{\alpha}h_{CB,n}y_n + w_{CB,n}, & \text{if } 1 \leq n \leq \Theta, \\ \sqrt{1-\alpha}h_{AD,n}x_n + h_{CB,n}t_n + w_{CB,n}, & \text{if } \Theta + 1 \leq n \leq L - \Theta, \\ \sqrt{1-\beta^\dagger}h_{AD,n}x_n + \sqrt{\beta^\dagger}h_{CB,n}s_n + w_{CB,n}, & \text{if } L - \Theta + 1 \leq n \leq L, \end{cases} \quad (34a)$$

$$\sqrt{1-\alpha}h_{AD,n}x_n + h_{CB,n}t_n + w_{CB,n}, \quad \text{if } \Theta + 1 \leq n \leq L - \Theta, \quad (34b)$$

$$\sqrt{1-\beta^\dagger}h_{AD,n}x_n + \sqrt{\beta^\dagger}h_{CB,n}s_n + w_{CB,n}, \quad \text{if } L - \Theta + 1 \leq n \leq L, \quad (34c)$$

where $\alpha = 1 - \Delta N_o$. Let $v_{n_1,CB}$, $v_{n_2,CB}$, and $v_{n_3,CB}$ denote the RVs corresponding to $|r_{D,CB,n_1}^\dagger|^2$, $|r_{D,CB,n_2}^\dagger|^2$, and $|r_{D,CB,n_3}^\dagger|^2$, respectively, such that $1 \leq n_1 \leq \Theta$, $\Theta + 1 \leq n_2 \leq L - \Theta$, and $L - \Theta + 1 \leq n_3 \leq L$. Thus, the RV corresponding to the average energy of L symbols on f_{CB} , denoted by $\mathcal{V}_{L,CB}$ is given as $\mathcal{V}_{L,CB} = \mathcal{V}_{L_1,CB} + \mathcal{V}_{L_2,CB} + \mathcal{V}_{L_3,CB}$, such that $\mathcal{V}_{L_1,CB} = \frac{1}{L} \sum_{n_1=1}^{\Theta} v_{n_1,CB}$, $\mathcal{V}_{L_2,CB} = \frac{1}{L} \sum_{n_2=\Theta+1}^{L-\Theta} v_{n_2,CB}$, and $\mathcal{V}_{L_3,CB} = \frac{1}{L} \sum_{n_3=L-\Theta+1}^L v_{n_3,CB}$. Using $\mathcal{V}_{L,CB}$, we formally define probability of miss-detection at Dave when measuring the average energy level on f_{CB} .

Definition 4. Given \mathcal{H}_1 is true, probability of miss-detection when Dave measures the average energy level on f_{CB} , denoted by $\mathbf{P}_{MD,CB}^{3\phi}$, is given as $\mathbf{P}_{MD,CB}^{3\phi} = \Pr(|\mathcal{V}_{L,CB} - \mathcal{E}_{CB}| \leq \nu_{CB} | \mathcal{H}_1 \text{ true})$.

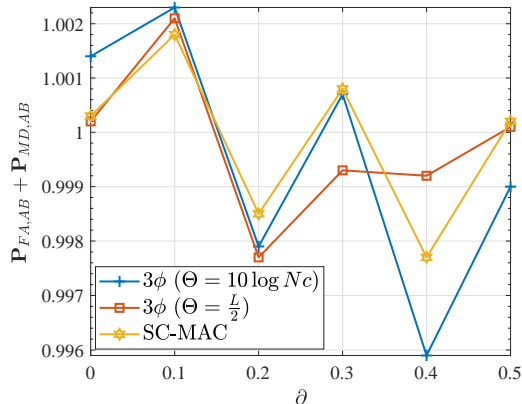
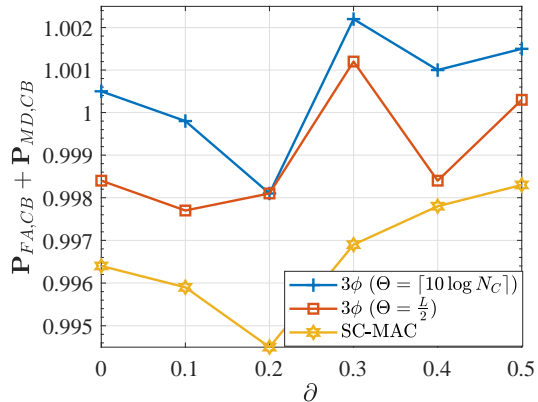
Proposition 1. When $N_o \ll 1$ and $\alpha = 1 - \Delta N_o$, the distributions of $\mathcal{V}_{L_1,CB}$ and $\mathcal{V}_{L_2,CB}$ are approximated as $\frac{1}{2^\Theta} \sum_{l=0}^{\Theta} \binom{\Theta}{l} G(l, \frac{1}{L})$ and $\frac{1}{2^{L-2\Theta}} \sum_{l=0}^{L-2\Theta} \binom{L-2\Theta}{l} G(l, \frac{1}{L})$, respectively. Thus, the distribution of $\frac{1}{L} \sum_{n=1}^{L-\Theta} |r_{D,CB,n}^\dagger|^2$ can be approximated as $\frac{1}{2^{L-\Theta}} \sum_{l=0}^{L-\Theta} \binom{L-\Theta}{l} G(l, \frac{1}{L})$.

From Proposition 1, we observe that the distribution of $|r_{D,CB,n}^\dagger|^2$ is approximately same as that of the distribution of $|r_{D,CB,n}|^2$, for $1 \leq n \leq L - \Theta$. This indicates that, Charlie solely controls the energy level on f_{CB} for the first $L - \Theta$ symbols after implementing 3ϕ DASC-MF scheme. However, during Phase-III, i.e., $L - \Theta + 1 \leq n \leq L$, Alice and Charlie use the energy-splitting factor β^\dagger away from 1, as shown in Table IV. Therefore, when Alice transmits a burst of zeros, the energy observed at Dave on f_{CB} is likely to be less than \mathcal{E}_{CB} , thereby resulting in higher probability of detection at Dave. Although, Alice and Charlie can choose to use β^\dagger close to 1, this will increase the fraction of erroneous decisions of Alice's current symbols.

While we are able to derive the probability of detection on f_{AB} , we do not derive closed-form expressions on probability of detection on f_{CB} , due to intractable density function contributed by Phase-III of the 3ϕ DASC-MF. However, we present simulation results on detection in Sec. VII-C.

B. Covertness Analysis for ED when using SC-MAC Scheme

Along the similar lines of Sec. VII-A, in this section, we define the probability of miss-detection at Dave on f_{AB} and f_{CB} , when Alice and Charlie use SC-MAC.

Fig. 11: $\mathbf{P}_{FA,AB} + \mathbf{P}_{MD,AB}$ on f_{AB} as a function of δ .Fig. 12: $\mathbf{P}_{FA,CB} + \mathbf{P}_{MD,CB}$ on f_{CB} as a function of δ .

Definition 5. The probability of miss-detection by Dave's ED on f_{AB} and f_{CB} are denoted by, $\mathbf{P}_{MD,AB}^{MAC}$ and $\mathbf{P}_{MD,CB}^{MAC}$, respectively. Further, $\mathbf{P}_{MD,AB}^{MAC} = \Pr(|\mathcal{W}_{L,AB} - \mathcal{E}_{AB}| \leq \nu_{AB} | \mathcal{H}_1 \text{ true})$ and $\mathbf{P}_{MD,CB}^{MAC} = \Pr(|\mathcal{W}_{L,CB} - \mathcal{E}_{CB}| \leq \nu_{CB} | \mathcal{H}_1 \text{ true})$, such that, $\mathcal{W}_{L,AB}$ and $\mathcal{W}_{L,CB}$ are the RVs denoting the average energy of L symbols received at Dave on f_{AB} and f_{CB} , respectively.

The distributions of $\mathcal{W}_{L,AB}$ and $\mathcal{W}_{L,CB}$ can be computed along the similar lines of $\mathcal{V}_{L,AB}$ and $\mathcal{V}_{L,CB}$, respectively. It is worthwhile to note that, since the entire frame of L symbols is uncoordinated in energy, the sum $\mathbf{P}_{FA,AB} + \mathbf{P}_{MD,AB}^{MAC}$ and $\mathbf{P}_{FA,CB} + \mathbf{P}_{MD,CB}^{MAC}$ should be away from 1, indicating that Dave is more likely to detect SC-MAC as compared to 3ϕ DASC-MF scheme.

C. Simulation Results

In this section, we provide results to showcase the covertness of the proposed schemes. In addition to the parameters used above, we use $\nu_{AB} = \nu_{CB} = 10^{-3}$. In Fig. 11, we first plot $\mathbf{P}_{FA,AB} + \mathbf{P}_{MD,AB}$ for both the proposed schemes as a function of δ at SNR = 25 dB, and observe that the sum is close to 1 for the considered range of δ . We also observe a similar behaviour in Fig. 12, where we plot $\mathbf{P}_{FA,CB} + \mathbf{P}_{MD,CB}$ for both the schemes. We note that, when $\Theta = \frac{L}{2}$, exactly $\frac{L}{2}$ symbols are transmitted in uncoordinated fashion, thus, $\mathbf{P}_{FA,CB} + \mathbf{P}_{MD,CB}$ is slightly higher than SC-MAC, where all the L symbols are uncoordinated in energy. However, since the 3ϕ DASC-MF scheme has minimum number of uncoordinated symbols, its $\mathbf{P}_{FA,CB} + \mathbf{P}_{MD,CB}$ is maximum and is close to 1 for all values of $\delta \in [0, 0.5]$.

VIII. CONCLUSION AND FUTURE WORK

This work presented a cooperative framework of delay-aware semi-coherent multiplex-and-forward scheme to mitigate an FD reactive jamming adversary. As a salient feature of this framework, the helper uses a practical FD radio to forward the victim's low-latency symbols to the destination. Here, the helper multiplexes the victim's symbols to its symbols to facilitate joint decoding at the destination. We first modelled the processing delay at the helper using a parameter, Θ and then

showed that the symbols received from the two users arrive during different symbol intervals at the destination, resulting in complex decoding. Further, we also pointed out that the symbols from both the users are uncoordinated in energy, leading to detection by an energy detector at the adversary. To circumvent these problems, we proposed two mitigation schemes based on the delay parameter Θ . When $\Theta \leq \frac{L}{2}$, we proposed 3ϕ delay-aware semi-coherent multiplex-and-forward scheme, wherein the legitimate users transmit their symbols using two energy-splitting factors, α and β , and the destination decodes them in three-phases, parametrised by Θ . We also proposed a semi-coherent multiple access channel scheme, when $\Theta > \frac{L}{2}$, wherein due to large Θ , the helper does not decode the victim's symbols, and the victim and the helper transmit their symbols to the destination using an energy-splitting factor, ε . For both the schemes, we provided near-optimal solution on the energy-splitting factor to the optimisation problem of minimising the error rates. Finally, we showed that the victim reliably communicates with the destination while adhering to the latency constraints without getting detected by the adversary.

There are multiple directions for future work. As part of the mitigation strategy against the *jam and measure* adversaries, non-coherent constellations can be designed in fast-fading channels when using delay-aware FD helper nodes. Also, throughout this work, we have assumed that the adversary can perfectly cancel its jamming energy on the victim's frequency bands. However, studying the impact of mitigation strategies with practical FD radios at the adversary is still an open problem.

REFERENCES

- [1] Y. Qian, F. Ye, and H.-H. Chen, *Security in 5G Wireless Networks*, 2022, pp. 279–310.
- [2] N. V. Huynh, D. T. Hoang, D. N. Nguyen, E. Dutkiewicz, and M. Mueck, “Defeating smart and reactive jammers with unlimited power,” in *2020 IEEE Wireless Communications and Networking Conference (WCNC)*, 2020, pp. 1–6.
- [3] V.-L. Nguyen, P.-C. Lin, B.-C. Cheng, R.-H. Hwang, and Y.-D. Lin, “Security and privacy for 6g: A survey on prospective technologies and challenges,” *IEEE Commun. Surveys Tut.*, vol. 23, no. 4, pp. 2384–2428, 2021.
- [4] D. Bharadia, E. McMillin, and S. Katti, “Full duplex radios,” in *Proc. of the ACM SIGCOMM 2013 Conf. on SIGCOMM*, 2013, pp. 375–386.
- [5] L. Anttila, V. Lampu, S. A. Hassani, P. P. Campo, D. Korpi, M. Turunen, S. Pollin, and M. Valkama, “Full-Duplexing with SDR Devices: Algorithms, FPGA Implementation, and Real-Time Results,” *IEEE Trans. on Wireless Commun.*, vol. 20, no. 4, pp. 2205–2220, 2021.
- [6] A. Sabharwal, P. Schniter, D. Guo, D. W. Bliss, S. Rangarajan, and R. Wichman, “In-band full-duplex wireless: Challenges and opportunities,” *IEEE J. on Sel. Areas in Commun.*, vol. 32, no. 9, pp. 1637–1652, 2014.
- [7] J. I. Choi, M. Jain, K. Srinivasan, P. Levis, and S. Katti, “Achieving single channel, full duplex wireless communication,” in *Proc. of the sixteenth Annu. Int. Conf. on Mobile Comput. and Netw.*, 2010, pp. 1–12.
- [8] A. Sahai, G. Patel, C. Dick, and A. Sabharwal, “Understanding the impact of phase noise on active cancellation in wireless full-duplex,” in *2012 Conf. Rec. of the Forty Sixth Asilomar Conf. on Signals, Syst. and Comput. (ASILOMAR)*. IEEE, 2012, pp. 29–33.
- [9] M. Jain, J. I. Choi, T. Kim, D. Bharadia, S. Seth, K. Srinivasan, P. Levis, S. Katti, and P. Sinha, “Practical, real-time, full duplex wireless,” in *Proc. of the 17th Annu. Int. Conf. on Mobile Comput. and Netw.*, 2011, pp. 301–312.

- [10] T. Riihonen, S. Werner, and R. Wichman, "Mitigation of loopback self-interference in full-duplex MIMO relays," *IEEE Trans. on signal Process.*, vol. 59, no. 12, pp. 5983–5993, 2011.
- [11] M. Amjad, F. Akhtar, M. H. Rehmani, M. Reisslein, and T. Umer, "Full-duplex communication in cognitive radio networks: A survey," *IEEE Commun. Surv. Tut.*, vol. 19, no. 4, pp. 2158–2191, 2017.
- [12] Y. Liao, L. Song, Z. Han, and Y. Li, "Full duplex cognitive radio: a new design paradigm for enhancing spectrum usage," *IEEE Commun. Mag.*, vol. 53, no. 5, pp. 138–145, 2015.
- [13] S. K. Sharma, T. E. Bogale, L. B. Le, S. Chatzinotas, X. Wang, and B. Ottersten, "Dynamic spectrum sharing in 5G wireless networks with full-duplex technology: Recent advances and research challenges," *IEEE Commun. Surv. Tut.*, vol. 20, no. 1, pp. 674–707, 2018.
- [14] X. Wang, M. Jia, Q. Guo, I. W.-H. Ho, and F. C.-M. Lau, "Full-duplex relaying cognitive radio network with cooperative nonorthogonal multiple access," *IEEE Syst. J.*, vol. 13, no. 4, pp. 3897–3908, 2019.
- [15] V. Chaudhary and J. Harshan, "Fast-forward relaying scheme to mitigate jamming attacks by full-duplex radios," in *2020 IEEE 31st Annual International Symposium on Personal, Indoor and Mobile Radio Communications*, 2020, pp. 1–7.
- [16] V. Chaudhary and H. Jagadeesh, "Fast-forward mitigation schemes for cognitive adversary," *IEEE Trans. Cogn. Commun. and Netw.*, vol. 7, no. 4, pp. 1304–1319, 2021.
- [17] V. Chaudhary and J. Harshan, "Non-coherent fast-forward relays for full-duplex jamming attack," in *2021 IEEE Global Communications Conference (GLOBECOM)*, 2021, pp. 1–6.
- [18] —, "Whisper when under attack: Delay tolerant fast-forward relays against full-duplex jamming," in *2022 14th International Conference on COMMunication Systems NETWORKS (COMSNETS)*, 2022, pp. 163–171.
- [19] V. Chaudhary and H. Jagadeesh, "Constellation design for non-coherent fast-forward relays to mitigate full-duplex jamming attacks," *IEEE Transactions on Communications*, pp. 1–1, 2022.
- [20] D. Bharadia and S. Katti, "Full duplex MIMO radios," in *11th USENIX Symposium on Networked Systems Design and Implementation (NSDI 14)*. USENIX Association, Apr. 2014, pp. 359–372.
- [21] —, "Fastforward: Fast and constructive full duplex relays," *ACM SIGCOMM Comput. Commun. Rev.*, vol. 44, no. 4, pp. 199–210, 2014.
- [22] G. Zheng, I. Krikidis, J. Li, A. P. Petropulu, and B. Ottersten, "Improving physical layer secrecy using full-duplex jamming receivers," *IEEE Trans. on Signal Process.*, vol. 61, no. 20, pp. 4962–4974, 2013.
- [23] J. Xu, L. Duan, and R. Zhang, "Proactive eavesdropping via cognitive jamming in fading channels," *IEEE Trans. on Wireless Commun.*, vol. 16, no. 5, pp. 2790–2806, 2017.
- [24] X. Hu, C. Kai, Z. Guo, and J. Gao, "A fast forward full-duplex cooperative relay scheme for securing wireless communications," *IEEE Signal Process. Lett.*, vol. 26, no. 5, pp. 775–779, 2019.
- [25] J. Harshan and Y.-C. Hu, "Cognitive radio from hell: Flipping attack on direct-sequence spread spectrum," in *2018 IEEE Wireless Commun. and Netw. Conf. (WCNC)*. IEEE, 2018, pp. 1–6.
- [26] H. Jagadeesh and Y.-C. Hu, "Convolution attack on frequency hopping by full-duplex radios," *IEEE Trans. Veh. Tech.*, vol. 68, no. 6, pp. 5642–5656, 2019.
- [27] M. K. Hanawal, D. N. Nguyen, and M. Krunz, "Cognitive networks with in-band full-duplex radios: Jamming attacks and countermeasures," *IEEE Trans. on Cogn. Commun. and Netw.*, vol. 6, no. 1, pp. 296–309, 2020.
- [28] 3GPP TS38.211, "NR; Physical Channels and Modulation," v15.3.0, Sept.2018.
- [29] M. Lichtman, R. P. Jover, M. Labib, R. Rao, V. Marojevic, and J. H. Reed, "LTE/LTE-A jamming, spoofing, and sniffing: threat assessment and mitigation," *IEEE Communications Magazine*, vol. 54, no. 4, pp. 54–61, 2016.
- [30] J. G. Proakis and M. Salehi, *Digital Communications*. McGraw-Hill Higher Education, 5th expanded ed., 2007.